# A New Approach to Grow High Quality Bulk $In_xGa_{1-x}As$ Crystal by Multi-component Zone Melting Method

**by**

**Mohammad Shaifur Rahman**

A thesis
Submitted to the Department of Electrical & Electronic Engineering,
Khulna University of Engineering & Technology (KUET) in partial
fulfillment of the requirements for the degree of
**Master of Science**
in
Electrical & Electronic Engineering

**December 2005**

**Department of Electrical & Electronic Engineering**
**Khulna University of Engineering & Technology (KUET)**
**Khulna-920300**

# A New Approach to Grow High Quality Bulk $In_xGa_{1-x}As$ Crystal by Multi-component Zone Melting Method

by

**Mohammad Shaifur Rahman**

A Dissertation Submitted to the Department of Electrical & Electronic Engineering, Khulna University of Engineering & Technology (KUET), in partial fulfillment of the requirements for the Degree of **Master of Science** in Electrical and Electronic Engineering is approved.

## Dissertation committee

**Dr. Md. Rafiqul Islam**
Associate Professor, Department of Electrical and Electronic Engineering,
Khulna University of Engineering and Technology, Khulna
Supervisor and Chairman

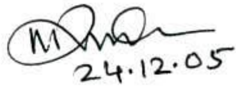

**Professor Dr. B. C. Ghosh**
Head, Department of Electrical and Electronic Engineering,
Khulna University of Engineering and Technology, Khulna

**Dr. Ashraful Ghani Bhuiyan**
Assistant Professor, Department of Electrical and Electronic Engineering,
Khulna University of Engineering and Technology, Khulna
Co-Supervisor

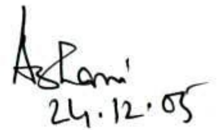

**Professor Dr. Abdur Rahim Mollah**
Department of Electrical and Electronic Engineering,
Ahsanullah University of Science and Technology, Dhaka

**Mr. A. N. M. Enamul Kabir**
Associate Professor, Department of Electrical and Electronic Engineering,
Khulna University of Engineering and Technology, Khulna

**Professor Dr. M. M. Shahidul Hassan**
Department of Electrical and Electronic Engineering,
Bangladesh University of Engineering and Technology, Dhaka

**Khulna University of Engineering & Technology**
Khulna-920300, Bangladesh.
December 2005

# Abstract

An analytical study has been carried out to grow high-quality bulk InGaAs crystals by the two-step multi-component zone melting (MCZM) method. Characterization of bulk InGaAs crystal grown by the two-step MCZM method has confirmed the existence of large amount of strain of the order of $10^{-2}$ in bulk InGaAs crystal due to approximately exponential variation of composition from 0.06 to 0.29 in the first step growth process of the two-step MCZM technique. From the experimental evidence, it has been confirmed that the composition-dependent strain is associated with the breakage issue in the MCZM grown crystals. Using an axially symmetrical strain model, the quantitative amount of strains and their distributions have been studied for various compositional profiles including the currently used profile. In addition, the spatial variations of strain components for various compositional profiles have been analyzed using the two-dimensional strain maps. The strain values and their distributions corresponding to the various compositional profiles have been compared and a suitable compositional profile has been proposed to grow compositionally homogeneous high quality bulk InGaAs crystals using the MCZM method. Further, from the dependency of the strain values with the crystal length and diameter, the possibility of the growth of large-size crystals has been investigated. It has also been studied that the proposed compositional profile allows achieving the growth parameters easily for the two-step MCZM growth process.

# Acknowledgement

I would like to gratefully acknowledge the enthusiastic supervision of Dr. Md. Rafiqul Islam during this work. His understanding, encouragement, motivation and expert guidance have provided a good basis for my entire research work. His overly enthusiasm and integral view on research and his mission for providing 'only high-quality work and not less', has made a deep impression on me. I owe him lots of gratitude for having me shown this way of research. He could not even realize how much I have learned from him.

I would also like to thank my co-supervisor Dr. Ashraful Ghani Bhuiyan who kept an eye on the progress of my work and was always available when I needed his advice. His stimulating suggestions and encouragement helped me in all the time of research work and writing this thesis.

I extend my sincere gratitude and appreciation to Dr. B. C. Ghosh, Dr. A. K. Azad, Dr. Monirul Islam, Mr. A. N. M. Enamul Kabir, Mr. Abdur Rafiq and Mr. Mohiuddin Ahmad who had been my course teachers during my graduate studies. I am indebted to all my faculty colleagues for their kind cooperation and providing me an excellent work environment during the past years.

I feel a deep sense of gratitude to my father and mother who formed part of my vision and taught me the good things that really matter in life. The sacred words of my father and mother always provide me a persistent inspiration for my journey in life.

Finally, my profound thanks go to the chairman and the members of the dissertation committee for their valuable comments which were supportive in enriching my thesis.

**Author**

# Contents

Abstract ........ i
Acknowledgement ........ ii
List of Figures ........ vi
List of Tables ........ x

**1. Introduction**

1.1 Back ground ........ 1
1.2 Growth History of Bulk $In_xGa_{1-x}As$ Crystals ........ 3
1.3 Growth Problems in Bulk $In_xGa_{1-x}As$ Crystals ........ 7
1.4 Motivation of Present Work ........ 8
1.5 Outline of Thesis ........ 9

**2. Strain in Bulk $In_xGa_{1-x}As$ Crystal Grown by MCZM Method**

2.1 Introduction ........ 11
2.2 Experimental Procedure ........ 12
2.3 Raman Results ........ 13
2.3.1 Raman Spectra in $In_xGa_{1-x}As$ Crystal ........ 13
2.3.2 $TO_{GaAs}$ Phonon Peaks and Lineshape Broadening ........ 15
2.4 Comparison between Raman and EDX Results ........ 16
2.5 Comparison between PL and EDX Results ........ 18
2.6 Quantitative Amount of Strain ........ 19
2.7 Summary ........ 22

**3. Evaluation of Strain under Compositional Variation in Bulk InGaAs Crystal**

3.1 Introduction ........ 24
3.2 One-dimensional Strain Model ........ 25
3.3 Axially Symmetrical Strain Model ........ 27
3.4 Analytical Solution of Strains in Cylindrical Co-ordinates ........ 28
3.5 Strain Distribution in Bulk $In_xGa_{1-x}As$ Mixed Crystals for Various

Compositional Profiles ........ 31
3.5.1 Strain Distribution for the Profiles AF, BF and CF ........ 33
3.5.2 Strain Distribution for the Profiles AE, BE and CE ........ 37
3.5.3 Strain Distribution for the Profiles AG, BG and CG ........ 39
3.6 Summary ........ 42

**4. Two-dimensional Mapping of Composition and Strain**
4.1 Introduction ........ 44
4.2 Two-dimensional Composition and Strain Maps ........ 45
4.2.1 Maps for the Profiles AE, BE and CE ........ 45
4.2.1.1 Composition Maps ........ 45
4.2.1.2 Axial Strain Maps ........ 46
4.2.1.3 Radial Strain Maps ........ 46
4.2.1.4 Tangential Strain Maps ........ 47
4.2.1.5 Shear Strain Maps ........ 47
4.2.1.6 Resultant Radial Strain Maps ........ 48
4.2.2 Maps for the Profiles AG, BG and CG ........ 51
4.2.2.1 Composition Maps ........ 51
4.2.2.2 Axial Strain Maps ........ 52
4.2.2.3 Radial Strain Maps ........ 52
4.2.2.4 Tangential Strain Maps ........ 53
4.2.2.5 Shear Strain Maps ........ 53
4.2.2.6 Resultant Radial Strain Maps ........ 54
4.2.3 Maps for Profiles AF, BF and CF ........ 55
4.2.3.1 Composition Maps ........ 55
4.2.3.2 Axial Strain Maps ........ 56
4.2.3.3 Radial Strain Maps ........ 57
4.2.3.4 Tangential Strain Maps ........ 57
4.2.3.5 Shear Strain Maps ........ 58
4.2.3.6 Resultant Radial Strain Maps ........ 58
4.3 Selection of the Best Profile ........ 60
4.4 Dependence of Strain with Crystal Length ........ 61

4.5 Dependence of Strain with Crystal Diameter .................... 63
4.6 Temperature Profiles .................... 66
4.7 Summary .................... 67

**5. Conclusions and Suggestions**
5.1 Conclusions .................... 69
5.2 Suggestions of future Works .................... 72

Bibliography .................... 73
List of Publications .................... 78

# List of Figures


| | | |
|---|---|---|
| 1.1 | A schematic of the two-step MCZM growth process. | 5 |
| 1.2 | a) Optical microscopic picture of the cut-surface of the InGaAs crystal that was cut along the diameter. The white circles indicate experimental points. b) Compositional variation measured by EDX experiments. | 6 |
| 1.3 | Phase diagram of InGaAs. | 7 |
| 2.1 | Raman spectra measured at room temperature along the centerline of a semi cylindrical $In_xGa_{1-x}As$ sample. The spectrum indicated by solid circles is obtained near the seed-crystal interface (seed-side) and the other spectra from the bottom to the top indicated by open circles are obtained from the interface (crystal-side) to the tail end of the sample, respectively. Inset shows an example of lineshape fitting where dotted curves represents different Lorentzian components. The peak corresponding to the disorder mode is shown by 'DM'. | 14 |
| 2.2 | Variation of a) $TO_{GaAs}$ peak positions and b) line-width as a function of the crystal length. | 16 |
| 2.3 | A comparison between the Raman and EDX data. The right hand scale is matched to the left hand scale using the compositional dependence of $TO_{GaAs}$ peak; $TO_{GaAs}(x) = 268 - 30x$, which was reduced in various polycrystalline $In_xGa_{1-x}As$ samples [15]. | 17 |
| 2.4 | A comparison between the PL and EDX data. The right hand scale is matched to the left hand scale using the compositional dependence of $E_g$; $E_g(x) = 1.424 - 1.56x + 0.494x^2$, which was measured at room temperature in | 18 |

unstrained $In_xGa_{1-x}As$ polycrystalline samples [26].

2.5 Variation of $TO_{GaAs}$ phonon peak along the diameter of the crystal at 16 mm and 21 mm length from the seed-crystal interface. 20

3.1 Lattice spacing change by the exponential-like compositional variation along the $z$ axis and parabolic compositional variation along the $r$ axis. 27

3.2 Typical compositional profiles a) along the growth direction, b) along the radial direction of the crystal. Actual profile may be any combination of the profiles A, B, or C with the profiles E, F, or G. 32

3.3 Strain distributions along the length of a cylindrical-shaped bulk InGaAs crystal for the compositional profiles AF, BF and CF at three different radial positions [centre ($r' = 0$), between centre and periphery ($r' = 0.5$) and periphery ($r' = 1$)]. 34

3.4 Strain distributions along the length of a cylindrical-shaped bulk InGaAs crystal for the compositional profiles AE, BE and CE at three different radial positions [centre ($r' = 0$), between centre and periphery ($r' = 0.5$) and periphery ($r' = 1$)]. 37

3.5 Strain distributions along the length of a cylindrical-shaped bulk InGaAs crystal for the compositional profiles AG, BG and CG at three different radial positions [centre ($r' = 0$), between centre and periphery ($r' = 0.5$) and periphery ($r' = 1$)]. 40

4.1 Composition maps for the profiles AE, BE and CE. 45

4.2 Axial strain maps for the profiles AE, BE and CE. 46

| | | |
|---|---|---|
| 4.3 | Radial strain maps for the profiles AE, BE and CE. | 46 |
| 4.4 | Tangential strain maps for the profiles AE, BE and CE. | 47 |
| 4.5 | Shear strain maps for the profiles AE, BE and CE. | 47 |
| 4.6 | Resultant radial strain maps for the profiles AE, BE and CE. | 48 |
| 4.7 | Composition maps for the profiles AG, BG and CG. | 51 |
| 4.8 | Axial strain maps for the profiles AG, BG and CG. | 52 |
| 4.9 | Radial strain maps for the profiles AG, BG and CG. | 52 |
| 4.10 | Tangential strain maps for the profiles AG, BG and CG. | 53 |
| 4.11 | Shear strain maps for the profiles AG, BG and CG | 53 |
| 4.12 | Resultant radial strain maps for the profiles AG, BG and CG. | 54 |
| 4.13 | Composition maps for the profiles AF, BF and CF. | 56 |
| 4.14 | Axial strain maps for the profiles AF, BF and CF. | 56 |
| 4.15 | Radial strain maps for the profiles AF, BF and CF. | 57 |
| 4.16 | Tangential strain maps for the profiles AF, BF and CF. | 57 |
| 4.17 | Shear strain maps for the profiles AF, BF and CF. | 58 |
| 4.18 | Resultant radial strain maps for the profiles AE, BE and CE. | 58 |
| 4.19 | Strain distributions of two crystals having 30 mm and 50 mm length with the same diameter (15 mm). | 62 |
| 4.20 | Strain distributions of two crystals having 20 mm and 15 mm diameter with equal length of 30 mm. | 64 |
| 4.21 | Strain distributions of two crystals having 30 mm length and 20 mm diameter and 60 mm length and 25 mm diameter. | 65 |

4.22 Solidification temperature profiles as a function of composition as well as normalized crystal length for the existing-like (AF) and proposed-like (CF) compositional profiles. 66

# List of Tables


2.1 TO phonon deformation potential for binary materials GaAs and InAs corresponding to <100> direction. 21

3.1 Physical constants in GaAs and InAs crystals [33]. 33

3.2 Maximum strain values at the three different radial positions ($r' = 0$, $r' = 0.5$, and $r' = 1$) for the compositional profiles AF, BF, and CF. 35

3.3 Maximum strain values at the three different radial positions ($r' = 0$, $r' = 0.5$, and $r' = 1$) for the compositional profiles AE, BE, and CE. 38

3.4 Maximum strain values at the three different radial positions ($r' = 0$, $r' = 0.5$, and $r' = 1$) for the compositional profiles AG, BG, and CG. 41

Chapter 1

# Introduction

## 1.1 Background

The progress of information technology has been very rapid, as can be seen from the recent worldwide expansion of use of the internet and cellular phones. The total information transmission volume consists of contributions by various medias, including printed matters, such as newspapers and journals, and the contributions from electro-communication technology, including television and radio broadcasting, telecommunications, and data communications [1]. In order to transmit these huge volumes of information, optical communication technology is being used since the early 1980s [2], where the key components are lasers and photodiodes. To meet the future demand of information society, development of high-speed, high-capacity, low-dispersion, and low-transmission-loss optical communication technology is highly demanded. However, for high efficient optical transmission systems, the key communication devices such as lasers and photodiodes should operate in the long wavelength region ranging from 1.3 to 1.55 μm [3]. The lasers and photodiodes operating in the wavelength range 1.3 to 1.55 μm are usually fabricated (InGaAs/InP, InGaAsP/InP) on InP substrate. Since the lattice constant of binary substrates is fixed, the optoelectronic properties of InP-based devices can not be controlled freely. Further, the lasing characteristics of semiconductor lasers (InGaAs/InP, InGaAsP/InP), operating at longer wavelengths of 1.3 to 1.5 μm, are

strongly dependent on temperature more than the semiconductor lasers (InGaAs/GaAs) operating at the shorter wavelengths ranging from 0.4 to 1.0 μm [4]. If ternary bulk crystals were used as substrates instead of binary crystals that are currently being used for fabricating various optoelectronic devices, the optical, electronic and mechanical properties of the devices can be tuned by choosing a proper value of composition, $x$, of the materials. Since the lattice parameter of ternary bulk substrate can be adjusted by the compositional fraction, $x$, such a substrate enables us to fabricate lattice-matched as well as controlled lattice-mismatched devices. Consequently, device performance and its life time would be improved.

Ternary compound bulk semiconductor materials such as $In_xGa_{1-x}As$ are promising and attractive lattice-matched substrate material for fabricating high performance laser diodes, which can be used as a light source in future optical access system. Ishikawa [5] theoretically predicted that the semiconductor lasers fabricated on $In_{0.3}Ga_{0.7}As$ substrates exhibit laser oscillation at 1.3 μm wavelength with high gain and improved temperature characteristics compared to the conventional InP-based laser diodes. Otsubo et al. [6] experimentally demonstrated that the temperature characteristics of InGaAs-based lasers were improved than InP-based lasers. However, gain characteristics were not improved since the crystal quality of the substrate was poor. In order to fabricate a wide variety of high-performance devices, large-size high-quality InGaAs single crystal with homogeneous composition is required. Several growth methods have been applied to grow such crystal but large-size single crystal with homogeneous composition could not be obtained. The crystals are often cracked and polycrystallized during the growth and cooling process, particularly, when the crystals are grown near the composition, $x \sim 0.3$. Therefore, it is very important to solve these issues for the potential applications of ternary bulk InGaAs crystals as

substrates in various optoelectronic devices.

## 1.2 Growth History of Bulk $In_xGa_{1-x}As$ Crystals

To the best of our knowledge Bonner et al. [7] for the first time tried to grow compositionally homogeneous InGaAs bulk crystals on GaAs seed using liquid encapsulated Czochralski (LEC) technique. However, the composition in the crystals obtained by this technique was varied from 0.02 to 0.05 and from 0.05 to 0.12 from the seed crystal. In the LEC growth process, the crystals are grown by cooling the InGaAs melt without melt replenishment. Consequently, there is no controllability of composition at the solid-liquid interface. In order to improve the controllability of the supply of GaAs to the melt close to the growing interface in LEC growth technique and hence to grow uniform and larger InGaAs ternary bulk crystals, Nakajima et al. [8] developed the double crucible LEC method. Using this improved LEC technique, it was possible to grow $In_{0.07}Ga_{0.93}As$ homogeneous bulk crystal with 5 cm in length and 1.5 cm in diameter.

Although Nakajima et al. were succeeded to grow $In_xGa_{1-x}As$ bulk crystals with homogeneous composition at $x \sim 0.07$ using double crucible LEC method, compositional inhomogeneity and crystal breakage issues became the key limiting factors to have homogeneous InGaAs crystals when the composition was increased above 0.07. It is anticipated that this breakage issue may be related with strain which is induced by changing lattice constant when InGaAs crystals with higher composition is grown on GaAs seed. It is believed that if ternary InGaAs crystals are used as seed, large-size $In_{0.3}Ga_{0.7}As$ with homogeneous composition could be obtained. Based on this idea, compositionally graded bulk $In_xGa_{1-x}As$ ($x = 0.05$ to 0.3) single crystals were grown by Nakajima et al. [9] using Bridgman method. Although the size of the crystal was 1.5 cm in length and 1.5 cm in diameter, the quality of the crystal was poor due to breakage. Thus, the InGaAs crystal grown by the conventional Bridgman method was not suitable

to use as seed for the growth of high quality large-size single crystals with uniform composition.

Later on, using vertical gradient freeze (VGF) method Nishijima et al. [10] have succeeded to grow bulk InGaAs single crystals on GaAs seed with good reproducibility. It was possible to obtain InGaAs single crystals with only 15 mm in length and 15 mm in diameter using this method, but the crystal quality was poor due to breakage and compositional inhomogeneity.

It is a dream of the crystal researchers to grow InGaAs single crystal with InAs composition, $x$ ~0.3, as the crystals with this composition are in high demand due to their uses in various light emitting and communication devices. In this connection, continuous efforts have been given for developing a suitable technique. Recently, Kinoshita et al. [11] have developed a new crystal growth method named as the traveling liquidus-zone (TLZ) method, which is the modified form of the vertical Bridgman method. Using TLZ method it was possible to grow $In_{0.3}Ga_{0.7}As$ single crystal with 20 mm in length, but its diameter was only 2 mm, which is not suitable for its practical use as substrate. This method was further applied to grow InGaAs crystals with 5 to 10 mm in diameter. But single crystal was not obtained. Because, when the crystal diameter is increased, convection-induced supercooling initiated the polycrystalline growth in the TLZ method.

To overcome the difficulties in growing InGaAs crystals a new crystal growth method named as multi-component zone melting (MCZM) method was further developed. MCZM method allows the reduction of temperature fluctuations caused by buoyancy and convection by reducing the liquid volume. Using the MCZM method Suzuki et al. [12] grew compositionally graded InGaAs single crystals without sample movement, and Nakajima et al. [8] grew compositionally homogeneous polycrystalline $In_{0.3}G_{0.7}aAs$ using

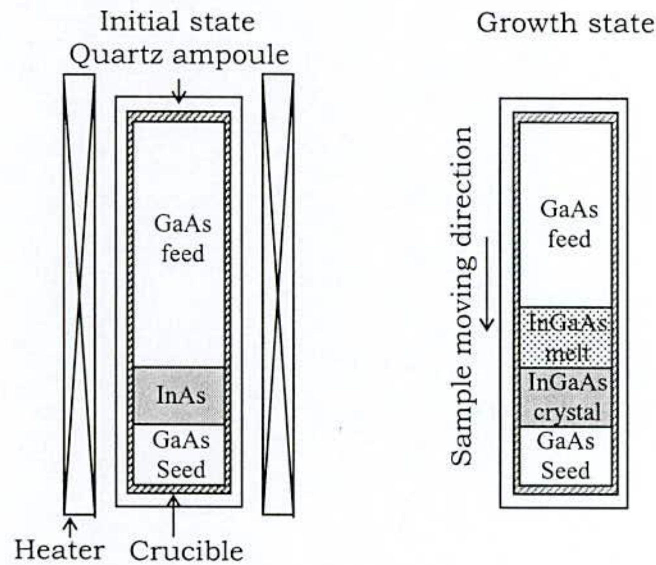


**Fig. 1.1:** A schematic of the two-step MCZM growth process.

sample movement or gradual cooling. Kodama et al. [13] developed the two-step MCZM method by modifying the conventional MCZM method. Using this method they were succeeded to grow compositionally homogeneous $In_{0.3}G_{0.7}aAs$ single crystal with larger diameter (15 mm), but the length was limited to only 4 mm due to breakage and polycrystallization. In the two-step MCZM method, composition in the crystal is gradually increased from the GaAs seed up to a certain value in the initial step and then it is kept constant at this value in the next step.

Figure 1.1 shows the schematic of the MCZM growth process. An InAs polycrystal is sandwiched between a GaAs seed crystal and a GaAs feed crystal as shown in Fig 1.1. The seed and feed (GaAs) crystals and the InAs polycrystal are all cylindrical in shape. The crystals are set in a pyrolytic boron nitride crucible and then sealed in quartz ampoule in a vacuum of under $8 \times 10^{-5}$ Pa. The sample is put in a vertical gradient heating furnace with the seed placed at the bottom. After annealing at 930 °C, the temperature at the growth interface is increased to the growth temperature of 1180 °C keeping the temperature gradient of the furnace constant at 15 °C/cm. When

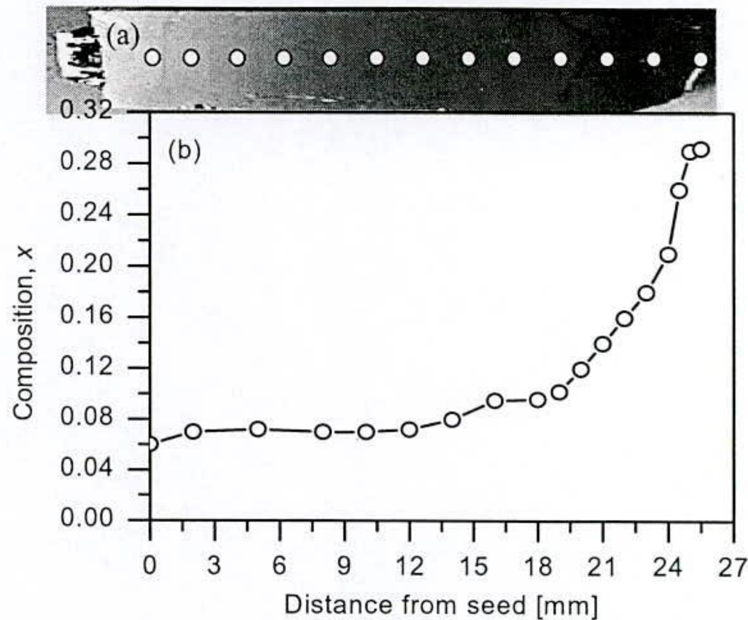


**Fig. 1.2:** Compositional variation measured by EDX experiments in the growth direction of the crystal grown by MCZM growth technique. Cross section along the growth length of the crystal is shown at the top.

the temperature exceeds 942 °C (the melting point of InAs), the surfaces of the GaAs crystals next to the InAs dissolve into the InAs melt and a ternary melt is formed. As known from the InGaAs phase diagram, the GaAs composition near the feed region becomes denser than that near the seed region because of the temperature difference. This difference in composition causes GaAs to diffuse towards the seed crystal, resulting in excess GaAs at the growth interface and ternary crystal grows on the surface of the seed crystal. The ternary composition of the grown crystal is determined in principle by the temperature at the growth interface. During the first step of the two-step MCZM growth process the InAs composition is gradually increased by moving the sample downward at a rate of 0.1 mm/h and reducing the furnace temperature to 1030 °C. In the next step, the InAs content of the growing crystal is kept constant by maintaining the temperature constant at the growth interface and moving the sample downward at the same rate. After growth and cooling

processes, the crystals are taken out from the crucible. Several cracked lines are usually found in MCZM crystals after certain growth length from the seed-crystal interface. To determine the compositional variation along the growth direction of the InGaAs crystal and hence to understand the cracking issue energy dispersive X-ray (EDX) measurement was performed at the centerline along the growth direction of the crystal. The result is shown in Fig. 1.2(b).

## 1.3 Growth Problems in Bulk $In_xGa_{1-x}As$ Crystals

Although the laser diodes fabricated on bulk $In_{0.3}Ga_{0.7}As$ showed outperform characteristics than the laser diodes fabricated on InP substrates, till now it is a great challenge for the crystal growers to grow compositionally homogeneous high-quality large-size single crystals, especially, near the composition $x \sim 0.3$. Because, there is a large discrepancy between the composition of InGaAs melt and its solidified form as can be seen in the InGaAs phase diagram in Fig. 1.3. It is found in Fig. 1.3 that if an InGaAs melt having more than

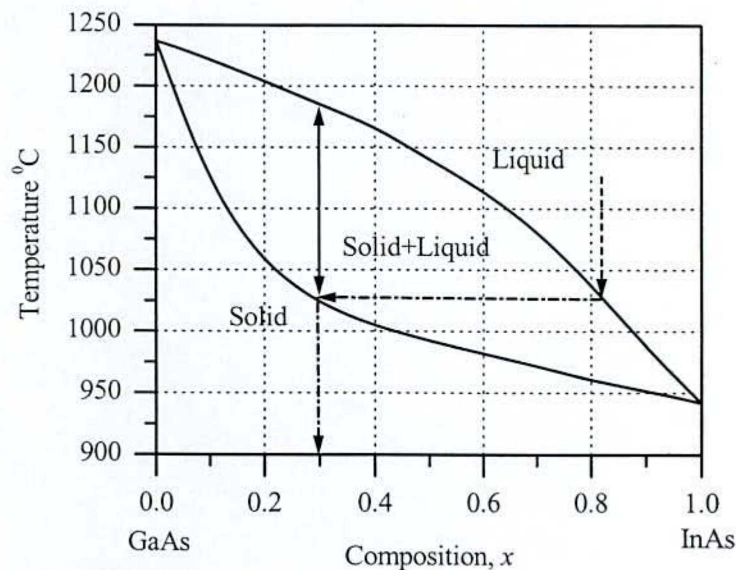


**Fig. 1.3:** Phase diagram of InGaAs

80% In-content is solidified at 1030 °C temperature, the In-content of the solidified material would be 30%. This is due to the fact that there is a large separation between the solidus and liquidus lines in the InGaAs phase diagram at this composition as shown in Fig. 1.3. In order to obtain crystals with homogeneous composition, it is required to maintain uniform composition at the solid-liquid interface. This is very difficult, because the melt composition at the solid-liquid interface changes by gravity-induced convection. Moreover, the influence of segregation due to the difference in diffusion constant between the In and Ga atoms lead to make large compositional inhomogeneity at the interface. Thus, the convection combined with the segregation at the time of solidification causes compositional variation in the grown crystal. The compositional inhomgeneity becomes more pronounced in the solidified material when the crystals are grown at composition $x \sim 0.3$, which may be due to the large temperature difference between the solidus and liquidus phases of InGaAs materials at this composition as indicated in Fig. 1.3.

## 1.4 Motivation of Present Work

The main objective in this study is to grow high quality bulk InGaAs crystal using the MCZM method. Up to now, LEC, vertical gradient freeze (VGF), Bridgman, TLZ and MCZM methods have been applied to grow bulk InGaAs crystals, but large size single crystal with homogeneous composition at about $x \sim 0.3$ could not be obtained. So far we know, bulk InGaAs crystals with homogeneous composition ($x \sim 0.3$) having 15 mm in diameter were possible to grow by the MCZM method. However, the crystal length was limited to only 4 mm due to breakage. It is expected that MCZM method can be used to grow high quality large-size crystals if the breakage issue could be solved. Some recent studies suggested that residual strain is induced in bulk mixed crystal under compositional variation and its amount and distribution

are highly sensitive to the compositional profiles. Since the composition at the first step of the MCZM growth process is increased gradually up to $x \sim 0.3$, the change in lattice spacing caused by compositional variation lead to induce mechanical strain. This composition-dependent mechanical strain is believed to be the main cause of crystal breakage in the MCZM growth process. Since the state of strain and its amount are highly dependent on compositional profile in bulk mixed crystals [14], there is a possibility to find out a suitable compositional profile, which can be used in the first step growth process in order to obtain high quality bulk InGaAs crystals using the two-step MCZM method. Based on this idea, the present study has been carried out to investigate the strain distribution and its magnitude for various compositional profiles. In addition, to find out a suitable compositional profile, two-dimensional mapping of strain has been developed for studying the spatial variation of strain in the entire regions of the crystal. By comparing the state of the strains and their distributions for various compositional profiles, the suitable compositional profile can be selected for the MCZM growth process.

In a word, the purpose of this research is to suggest the suitable compositional profile, which would solve the breakage issue in the two-step MCZM growth technique. It is expected that the outcome of the present research would provide useful information in semiconductor industry for growing high-quality, large-size bulk InGaAs crystals using the MCZM method.

## 1.5 Outline of Thesis

Chapter 1 includes the background and motivations of this research work. In this chapter, the applications of ternary bulk InGaAs substrates for fabricating high performance devices have been

discussed. The growth history and the problems pertaining to the growth of large-size high-quality $In_xGa_{1-x}As$ single crystals have been described. The issue remained to be solved to have compositionally homogeneous large-size $In_xGa_{1-x}As$ single crystals using the two-step MCZM growth technique have been focused.

In chapter 2, existence of strain in bulk InGaAs crystals grown by the two-step MCZM method has been confirmed by means of Raman scattering (RS), photoluminescence (PL) and energy dispersive X-ray (EDX) experiments. At the first part of this chapter, appropriateness of the combination of EDX measurement with the RS and PL measurements for investigating the strain in bulk $In_xGa_{1-x}As$ mixed crystal has been justified. Next, a series of experimental results have been presented for confirming the existence of residual strain in bulk InGaAs crystal grown by the two-step MCZM method.

In chapter 3, an axially symmetrical strain model has been applied to evaluate the quantitative amount of strains and hence to understand their distributions for various compositional profiles in bulk InGaAs crystals. The dependence of strain values with the compositional profiles has also been presented.

In chapter 4, two-dimensional mapping of strain and composition have been developed. Comparing the strain maps, a better compositional profile has been selected for the MCZM growth process to grow large-size high-quality InGaAs crystals. Further, the dependence of strain values with the crystal length and diameter has also been explained.

Chapter 5 provides the conclusions of the present research and the prospects for the future studies.

# Chapter 2

# Strain in Bulk $In_xGa_{1-x}As$ Crystal Grown by Two-step MCZM Method

## 2.1 Introduction

It is an interesting and challenging work to grow large-size high-quality bulk $In_{0.3}Ga_{0.7}As$ crystals with homogeneous composition. However, nobody has succeeded to grow such crystals, although several attempts have been made by using different crystal growth techniques. To the best of our knowledge, Kodama et al. [13] for the first time succeeded to grow bulk $In_{0.3}Ga_{0.7}As$ crystals with 15 mm in diameter using the two-step MCZM method. But the crystal length was limited to only 4 mm due to breakage. It is anticipated that this breakage issue may be associated with strain induced by the compositional variation at the first step growth of bulk InGaAs crystal in the two-step MCZM growth process. In order to investigate the existence of strain in the crystal grown by the two-step MCZM method, Raman scattering (RS), photoluminescence (PL) and energy dispersive X-ray (EDX) experiments have been performed.

Both RS and PL are nondestructive efficient ways to investigate composition and strain in semiconductor materials. The shift in optical phonon in Raman spectra originates form the absolute change in composition for unstrained crystals [15]. However, in the presence of strain, phonon positions contain composition-dependent shift as well as strain-induced shift [16, 17]. Therefore, RS is a good

characterization technique to investigate the composition and residual strain. Similarly, luminescence peak position in PL spectra depends on strain and composition [18]. Although PL peak energy could be shifted slightly from the band gap energy of materials, PL spectrum is sharp enough to determine composition with high accuracy. By assuming the PL peak energy as band gap energy, the compositions evaluated in various unstrained polycrystalline materials were found to be deviated about 5% with those evaluated by standard chemical analysis [18]. In contrast to RS and PL measurements, EDX measurements have no influence of strain, which has already been established [19]. Therefore, a combination of EDX measurement with the RS and PL measurements could be a good way to investigate the strain in bulk $In_xGa_{1-x}As$ mixed crystal under investigation.

## 2.2 Experimental Procedure

Bulk $In_xGa_{1-x}As$ mixed crystals of 15 mm in diameter were grown with a (111) GaAs seed by the two-step MCZM method [13]. The crystal was cut into two semi-cylindrical pieces of samples along the growth length. The cut surface of one sample was mechanically polished and then EDX measurements were carried out at the centerline along the growth length to evaluate the compositional variation. The composition was found to increase gradually from 0.06 to ~ 0.29 from the seed-crystal interface up to a certain distance along the growth length of the sample.

RS measurements were also made at room temperature using a Ranishaw model 2000 micro-Raman system equipped with an argon-ion laser operating at $\lambda$ = 514.5 nm wavelength and a cooled CCD detector. The incident light was focused on the sample surface with a 50× objective lens and the scattered light was collected by the same lens. In the experiment, laser power was low enough to prevent the local heating and optical damages of the sample. In order to reduce

the Rayleigh scattering light and background noise, a suitable notch filter was used and slit width was reduced to about 100 μm.

In addition, using a PL mapping system equipped with a 17 mw He-Ne laser (λ = 632 nm) and a cooled InGaAs detector, PL measurements were performed at room temperature. The optical arrangement was similar to that of Raman scattering. Peak positions of PL spectra were determined by lineshape fitting.

## 2.3 Raman Results

### 2.3.1 Raman Spectra in $In_xGa_{1-x}As$ Crystal

First order Raman spectrum from a semiconductor typically shows LO and TO phonons. However, depending upon the crystal orientation and experimental geometry one of them may be optically forbidden [20]. The ternary compound semiconductor $In_xGa_{1-x}As$ shows two-mode behavior [15, 21-23] in the first-order Raman scattering, in which LO and TO phonons corresponding to both InAs and GaAs binary end materials are found. The appearance and frequency position of these phonons depend on the compositional fraction, $x$ [15, 23]. Figure 2.1 shows a series of Raman spectra measured along the centerline of the semi-cylindrical $In_xGa_{1-x}As$ sample. The spectrum shown by solid circles in Fig. 2.1 is from the seed-side near the seed-crystal interface. Other spectra from the bottom to the top shown by open circles are corresponding, respectively, from the crystal side near the seed-crystal interface to the tail-end of the sample. Since the spectra were measured from the (110) surface of the sample, $TO_{GaAs}$ phonon peak is found to be strong in the spectra. Besides the $TO_{GaAs}$ phonon peak, weak peaks corresponding to InAs and GaAs-like LO phonons are also observed in the spectra. Furthermore, an additional structure seems to be superimposed with $TO_{GaAs}$ peak whose intensity becomes more prominent than $TO_{GaAs}$ peak in the spectra measured near the tail-end

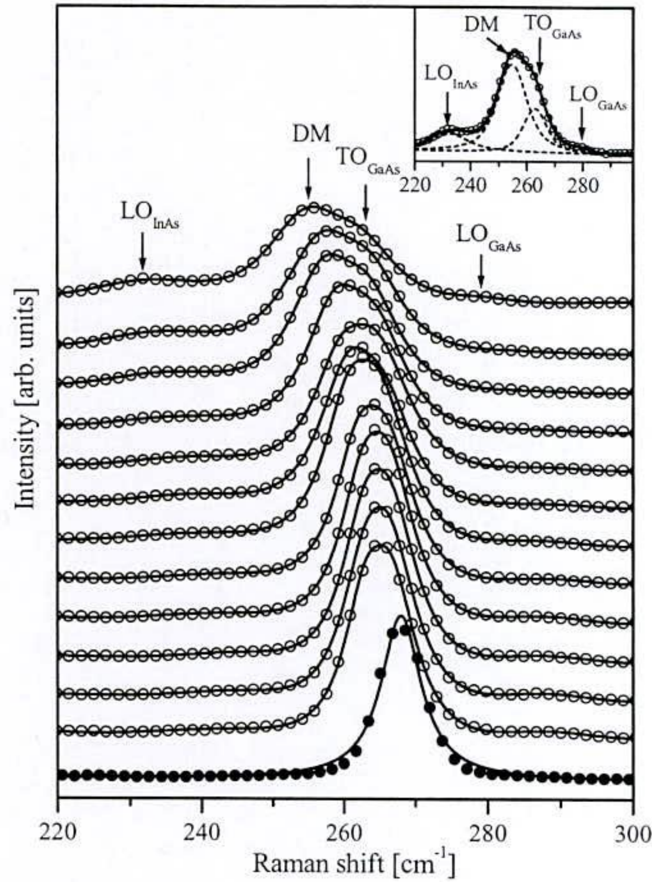


**Fig. 2.1:** Raman spectra measured at room temperature along the centerline of a semi cylindrical $In_xGa_{1-x}As$ sample. The spectrum indicated by solid circles is obtained near the seed-crystal interface (seed-side) and the other spectra from the bottom to the top indicated by open circles are obtained from the interface (crystal-side) to the tail end of the sample, respectively. Inset shows an example of lineshape fitting where dotted curves represents different Lorentzian components. The peak corresponding to the disorder mode is shown by 'DM'.

of the sample. Although the origin of this structure is not clear at the present stage, it seems to be disorder activated mode. The phonon dispersion may experience disorder with increasing In-content resulting in the appearance of disorder activated mode. Similar disorder mode was found in the Raman spectra measured from the

compound semiconductor materials $Si_{1-x}Ge_x$ [24]. As seen in Fig. 2.1 $TO_{GaAs}$ peak is shifted drastically to lower frequency direction in the spectrum measured from the crystal-side than that of the seed-side at the interface. However, $TO_{GaAs}$ peaks are found to be shifted gradually in the spectra, which were measured from the crystal-side near the interface to the tail-end of the sample. This shift in phonon positions demonstrates that there exists compositional variation in the crystal. In order to understand the tendency of the shift in phonons and their lineshape broadening, the spectra were best fitted using Lorentzian components and a proper background. An example of such lineshape fitting is shown in the inset of Fig 2.1.

### 2.3.2 $TO_{GaAs}$ Phonon Peaks and Lineshape Broadening

Figure 2.2(a) shows variation of $TO_{GaAs}$ peak positions as a function of crystal length where they are found to vary drastically at the seed-crystal interface. Apart from the interface, the $TO_{GaAs}$ peaks are varied gradually for a certain distance along the growth length and then varied drastically near the tail-end of the sample. The variation of $TO_{GaAs}$ peaks indicates the existence of compositional variation from the seed-end to the tail-end of the sample. Islam et al. suggested in a previous study [16, 17] that the shift in optical phonons is influenced by the strain under compositional variation in bulk mixed crystals. Therefore, the observed $TO_{GaAs}$ peak positions should have the influence of strain.

It was suggested in a previous study [25] that Raman lineshape is broadened due to strain, where the influence of strain on TO phonon is found to be more than that on LO phonon. Figure 2.2(b) shows the variation of linewidth of $TO_{GaAs}$ peaks as a function of the crystal length. It is observed in Fig. 2.2(b) that the linewidth of $TO_{GaAs}$ phonon changes drastically from 6.69 $cm^{-1}$ to 9.68 $cm^{-1}$ in the spectra measured from the seed-side to the crystal-side at the seed-crystal

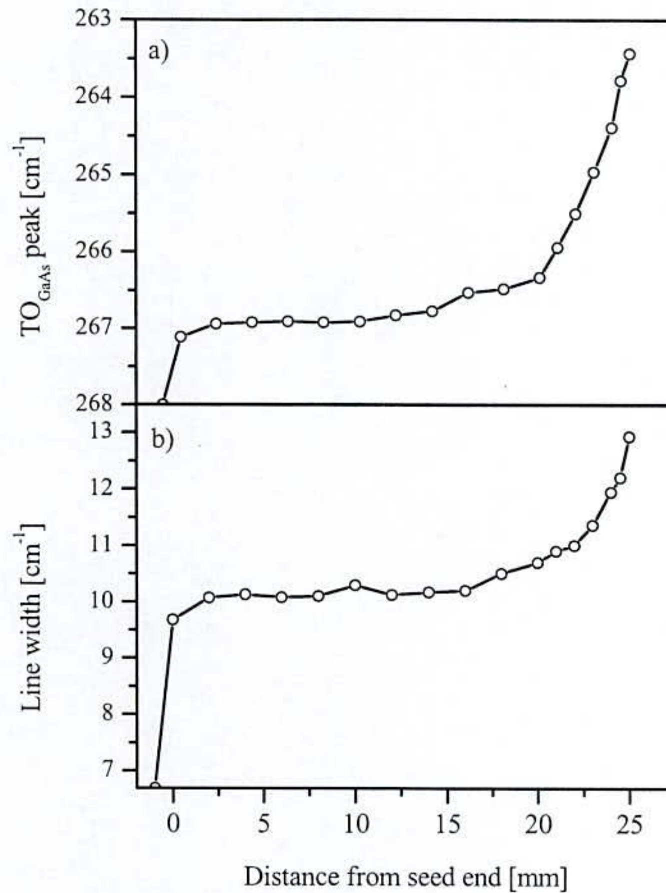


**Fig. 2.2:** Variation of a) $TO_{GaAs}$ peak positions and b) line-width as a function of the crystal length.

interface. This drastic change in linewidth may be associated with the strain induced by the step change in lattice spacing between the seed and crystal sides at the interface. The linewidth of $TO_{GaAs}$ phonon is then varied gradually from 9.68 to 12.93 cm$^{-1}$ from the seed-crystal interface to the tail-end of the sample, which could be due to strain induced by gradual change in lattice spacing due to the compositional variation.

## 2.4 Comparison between Raman and EDX Results

In order to confirm the influence of strain on $TO_{GaAs}$ peaks, a

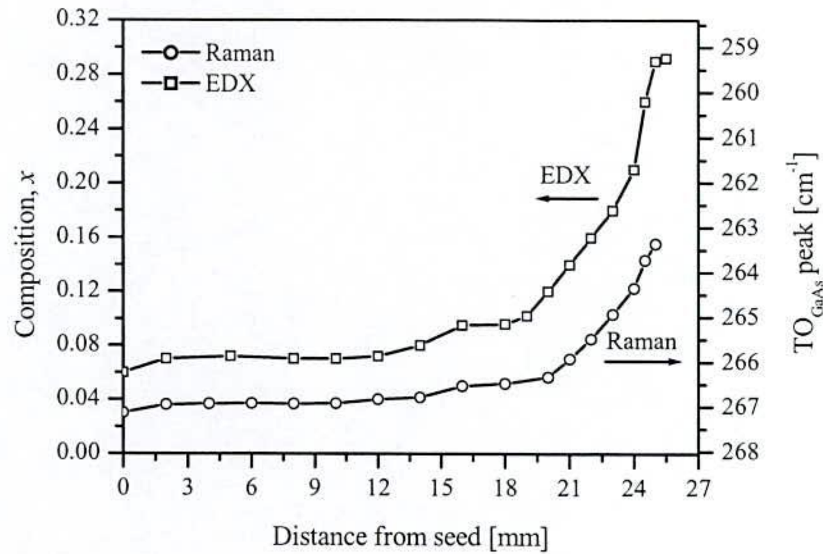


**Fig. 2.3:** A comparison between the Raman and EDX data. The right hand scale is matched to the left hand scale using the compositional dependence of $TO_{GaAs}$ peak; $TO_{GaAs}(x)$ = 268 – 30$x$, which was reduced in various polycrystalline $In_xGa_{1-x}As$ samples [15].

comparison between the Raman and EDX results is shown in Fig. 2.3. The left and right hand scales in Fig. 2.3 are corresponding to the EDX composition and $TO_{GaAs}$ peak positions, respectively. The right hand scale is matched to the left hand scale using the compositional dependence of $TO_{GaAs}$ phonon frequency: $TO_{GaAs}(x)$ = 268 - 30$x$, which was reduced in unstrained $In_xGa_{1-x}As$ polycrystalline materials in a previous study [15]. It is found in Fig. 2.3 that there is a big difference between the Raman and EDX results, which is found to increase from .9 to 4.04 $cm^{-1}$ with increasing composition from 0.06 to 0.29. It is well established that EDX measurements have no influence of strain. On the other hand, Raman peaks are influenced both by strain and composition [16, 17]. Therefore, it is confirmed that the discrepancy between Raman and EDX results is arisen due to the strain, which is induced by the compositional variation in the crystalline bulk

$In_xGa_{1-x}As$ grown by the MCZM method.

## 2.5 Comparison between PL and EDX Results

The existence of strain in the sample is further confirmed from a comparison between the PL and EDX results as shown in Fig. 2.4. The left hand scale of Fig. 2.4 shows EDX composition while the right hand scale shows PL peak energy position. The right hand scale is matched to the left hand scale using the compositional dependence of band gap energy: $E_g(x) = 1.424 - 1.56x + 0.494x^2$, which was reduced at room temperature in unstrained $In_xGa_{1-x}As$ materials in the past [26]. It is found in Fig. 2.4 that there is a large difference between the PL and EDX results, which increases with increasing composition. It is well known that the electronic energy bands are modified under the influence of strain. On the other hand, absolute value of composition can be obtained from the EDX measurement [13]. Therefore, the difference between the PL and EDX results arises due to the influence

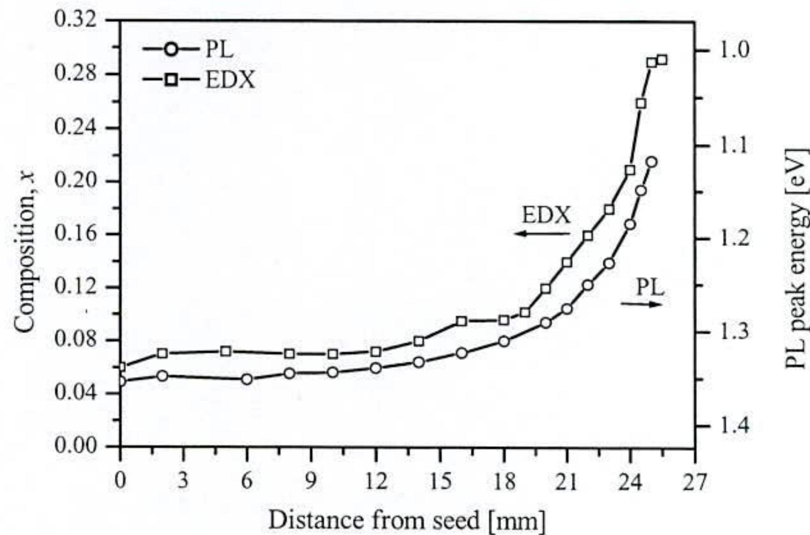


**Fig. 2.4:** A comparison between the PL and EDX data. The right hand scale is matched to the left hand scale using the compositional dependence of $E_g$; $E_g(x) = 1.424 - 1.56x + 0.494x^2$, which was measured at room temperature in unstrained $In_xGa_{1-x}As$ polycrystalline samples [26].

of strain on the PL results. The strain-induced change in PL peak energy is found to vary from 0.017 to 0.097 eV for the variation of composition from 0.06 to 0.29.

## 2.6 Quantitative Amount of Strain

It is difficult to separate out the strain contribution from the observed $TO_{GaAs}$ and PL peak positions as they are influenced both by strain and by composition. However, with the combination of RS, PL and EDX measurements, the strain contribution can be separated since EDX measurements have no influence of strain. By subtracting RS and PL data from the EDX data, the strain-induced shifts are evaluated to be 4.04 $cm^{-1}$ and 0.097 eV for the compositional variation from 0.06 to 0.29. If strain-induced shift is known, one can determine the amount of strain using the following relationships [14],

$$\Delta\Omega_1 = \frac{1}{2}\Big[\widetilde{K}_{12}\varepsilon_{zz} + \left(\widetilde{K}_{11}\cos^2\theta + \widetilde{K}_{12}\sin^2\theta\right)\varepsilon_{rr} + \left(\widetilde{K}_{11}\sin^2\theta + \widetilde{K}_{12}\cos^2\theta\right)\varepsilon_{\theta\theta} + \widetilde{K}_{44}\cos\theta\varepsilon_{rz}\Big]\Omega_0 \qquad (2.1)$$

$$\Delta\Omega_2 = \frac{1}{2}\Big[\widetilde{K}_{12}\varepsilon_{zz} + \left(\widetilde{K}_{11}\sin^2\theta + \widetilde{K}_{12}\cos^2\theta\right)\varepsilon_{rr} + \left(\widetilde{K}_{11}\cos^2\theta + \widetilde{K}_{12}\sin^2\theta\right)\varepsilon_{\theta\theta} + \widetilde{K}_{44}\sin\theta\varepsilon_{rz}\Big]\Omega_0 \qquad (2.2)$$

$$\Delta\Omega_3 = \frac{1}{2}\Big[\widetilde{K}_{11}\varepsilon_{zz} + \widetilde{K}_{12}\left(\varepsilon_{rr} + \varepsilon_{\theta\theta}\right) + \widetilde{K}_{44}\left(\cos\theta + \sin\theta\right)\varepsilon_{rz}\Big]\Omega_0 \qquad (2.3)$$

where $\Delta\Omega_1$, $\Delta\Omega_2$ and $\Delta\Omega_3$ are the strain-induced shifts for different phonon modes at the center of the Briluin zone. $\widetilde{K}_{11}$, $\widetilde{K}_{12}$ and $\widetilde{K}_{44}$ are the phonon deformation potentials in <100> direction of the crystal and $\Omega_0$ is the phonon frequency for unstrained crystals. $\varepsilon_{rr}$, $\varepsilon_{\theta\theta}$ and $\varepsilon_{zz}$ are the principal strain components in cylindrical coordinates along radial, tangential and axial direction, respectively. $\varepsilon_{rz}$ is the shear strain component.

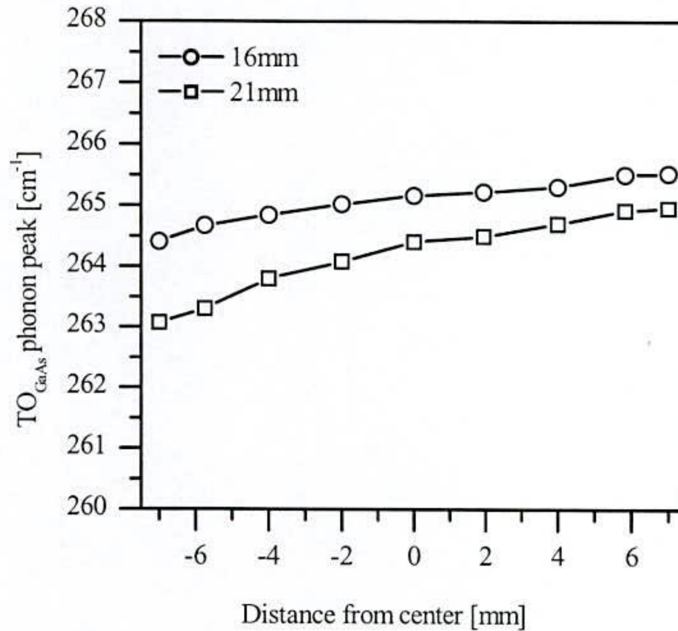


**Fig. 2.5:** Variation of $TO_{GaAs}$ phonon peak along the diameter of the crystal at 16 mm and 21 mm length from the seed-crystal interface.

In the present sample, the compositional profile was found to be about exponential along the growth direction. In order to investigate the compositional profile along the radial direction Raman measurements were also performed along the diameter at several points along the length of the crystal. The results are summarized in Fig. 2.5, where $TO_{GaAs}$ phonon peaks measured at 16 mm length along the radial direction are found to vary from 264.4 cm$^{-1}$ to 265.53 cm$^{-1}$. Similar results are found to vary from 263.07 cm$^{-1}$ to 264.96 cm$^{-1}$ at 21 mm crystal length from the seed-crystal interface. Thus the experimental results demonstrate that there exists compositional variation along the diameter of the crystal and it increases while moving from the seed-end to the tail end of the crystal. As a result all principle and shear strain components may exist in the sample and

**Table 2.1:** TO phonon deformation potential for binary materials GaAs and InAs corresponding to <100> direction.

| Material | $\widetilde{K}_{11}$ | $\widetilde{K}_{12}$ | $\widetilde{K}_{44}$ |
|---|---|---|---|
| GaAs | -2.4 | -2.7 | -0.9 |
| InAs | -2.053 | -2.62 | -0.75 |

their distribution would be complicated due to complex compositional profile. Hence, it is difficult to estimate the actual amount of strains in the sample investigated here.

In order to realize the strain value, if a simple one dimensional strain distribution is considered, the approximate amount of strain can be estimated for any phonon modes by equations 2.1 to 2.3. If $\varepsilon_{rr}$, $\varepsilon_{\theta\theta}$ and $\varepsilon_{rz}$ are assumed to be zero, these equations reduce to,

$$\Delta\Omega_1 \approx \frac{1}{2}\widetilde{K}_{12}\varepsilon_{zz}\Omega_0 \tag{2.4}$$

$$\Delta\Omega_2 \approx \frac{1}{2}\widetilde{K}_{12}\varepsilon_{zz}\Omega_0 \tag{2.5}$$

$$\Delta\Omega_2 \approx \frac{1}{2}\widetilde{K}_{11}\varepsilon_{zz}\Omega_0 \tag{2.6}$$

Using one of the above equations the approximate value of axial strain can be calculated. Since the probing laser beam was directed along <111> direction in the present experiment, the equations can be expressed as

$$\Delta\Omega(strain) \approx \frac{1}{2}\widetilde{K}'\varepsilon_{zz}\Omega_0 \tag{2.7}$$

where $\widetilde{K}'$ is the phonon deformation potential (PDP) along the growth axis of the crystal corresponding to the <111> growth direction. It is to be noted here that the binary components of PDP are available only for the <100> growth direction as listed in Table 2.1, whereas our

sample was grown in the <111> direction. Therefore, we calculated the appropriate values in the <111> growth direction using the tensor rotation technique.

$$\widetilde{K}'_{11} = \widetilde{K}'_{22} = \frac{1}{2}(\widetilde{K}_{11} + \widetilde{K}_{12} + 2\widetilde{K}_{44}) \tag{2.8}$$

$$\widetilde{K}'_{12} = \frac{1}{6}(\widetilde{K}_{11} + 5\widetilde{K}_{12} - 2\widetilde{K}_{44}) \tag{2.9}$$

So far we know there are no direct experimental measurements of PDPs in InGaAs alloy; therefore, PDP used in the present calculations was determined using the interpolation relation between the values estimated for the binary compounds. Using Eq. 2.7 the strain along the growth direction is estimated of the order of $10^{-2}$ corresponding to 4.04 $cm^{-1}$ strain-induced shift. This strain value is large enough to explain the breakage mechanism in bulk $In_xGa_{1-x}As$ crystals grown by the MCZM method. In fact, several cracked lines were observed at the tail-end of the crystal, which may be resulted from the high value of strain accumulated at the tail-end of the sample due to the gradual variation of the composition.

## 2.7 Summary

To investigate the residual strain induced by compositional variation in bulk $In_xGa_{1-x}As$ crystal grown by the MCZM method, RS, PL and EDX measurements have been carried out. It was found from a comparison among the RS, PL and EDX results that $TO_{GaAs}$ and PL peak positions were changed under the influence of strain. The strain-induced shift in phonon position was found to be 4.04 $cm^{-1}$ for the variation of composition from 0.06 to 0.29. Further, for the same range in composition, PL peak energy was changed approximately at

0.097 eV. Furthermore, the lineshape of $TO_{GaAs}$ phonon was broadened drastically approximately 2.99 $cm^{-1}$ near the seed crystal interface due to the drastic change in composition from 0 to 0.06. However, for the gradual change in composition from 0.06 to 0.29, the lineshape of the $TO_{GaAs}$ phonon was changed from 9.68 $cm^{-1}$ to 12.93 $cm^{-1}$. The broadening of phonon lineshape may also demonstrate the existence of strain in the sample. Although the exact amount of strain could not be evaluated due to complex strain distribution in the crystal, by assuming one-dimensional strain distribution, an approximate value of strain of the order of $10^{-2}$ was evaluated along the centerline of the sample for the variation of composition from 0.06 to 0.29. Therefore, such high value of strain induced by the compositional variation could be the cause of crystal breakage in the MCZM growth process. To understand the quantitative amount of strains and their distributions with various compositional profiles in the crystal grown by the MCZM method, an axially symmetrical strain model has been used. The results obtained from the model are discussed in the next chapter.

Chapter 3

# Evaluation of Strain under Compositional Variation in Bulk InGaAs Crystal

## 3.1 Introduction

In this chapter, strain models developed for bulk mixed crystal system have been applied to determine the quantitative amount of strains and their distributions for various compositional profiles in bulk InGaAs crystals grown by the two-step MCZM method. Further, the dependencies of strain values with the shape of the compositional profiles have been investigated.

Residual strain induced by compositional variation in bulk mixed crystals is a new issue and is very important for understanding the growth problems in bulk mixed crystal system. Islam et al. [14] suggested, by the combination of RS, PL, and EDX experiments, that residual strain is induced due to the compositional variation in bulk mixed crystals grown by the normal freezing method. Although the above experimental techniques can be used to investigate the existence of strain in bulk mixed crystals, the amount of strain can not be measured by them. Residual strain induced by the step change in lattice constant between the substrates and epilayers was extensively investigated using the well known epilayer strain models [27-30]. However, epilayer strain models can not be applied to

determine strain in bulk mixed crystal system. Because, strain phenomena in epilayer system are not the same with that of bulk mixed crystals. With an aim to understand the relationship between the strain and compositional variation in bulk mixed crystal system, a simple one-dimensional (1-D) strain model was proposed by Islam et al. [32], which can be applied to evaluate the axial strain component. In order to evaluate not only the axial strain component but also the radial, tangential and shear strain components in cylindrically-shaped bulk mixed crystal system with various compositional profiles, they further proposed an axially symmetrical strain model [14]. Since the composition is varied at the first step of the two-step MCZM growth process, the change in lattice spacing by the compositional variation may lead to induce residual strain in the crystal. Therefore, the breakage issue associated with the compositional variation in the bulk $In_xGa_{1-x}As$ crystals grown by the MCZM method can be investigated using the axially symmetrical strain model. In this chapter, the results obtained from the model for different compositional profiles have been presented.

## 3.2 One-dimensional Strain Model

A simple one-dimensional strain model can be applied to estimate the strain in bulk mixed crystals for simple strain distribution. However, it is not suitable to investigate strain components for complicated strain distribution. A 1-D model was described [32] by assuming an exponential variation of composition in the growth direction and homogeneous composition in the radial direction of a cylindrically-shaped crystal. In this model, the shear strain component is neglected along the growth axis of the crystal on account of axial symmetry.

In bulk mixed crystals, the lattice spacing changes continuously with the change in composition, therefore, strain in bulk crystal can be

expressed by

$$\varepsilon_{zz}(x) = \alpha_l x(z), \tag{3.1}$$

where $\varepsilon_{zz}(x)$ is the strain induced by compositional variation, $\alpha_l = \frac{1}{a(x)} \frac{da(x)}{dx}$ is the rate of change in lattice spacing, $a(x)$ is the compositional dependence of the lattice spacing, and $x(z)$ is the compositional variation along the growth direction of the crystal. If $\varepsilon_{zz}$ is the actual axial strain, then, $\varepsilon_{zz} - \varepsilon_{zz}(x)$ represents the part due to external stress. In one dimensional case, $\varepsilon_{rr} + \varepsilon_{\theta\theta} = -\varepsilon_{zz}$, where $\varepsilon_{rr}$ and $\varepsilon_{\theta\theta}$ are the strain components, respectively, along the radial and tangential directions in a cylindrical coordinate system. Using the ordinary stress-strain relationship [31], the stress along the growth direction can be given by

$$\sigma_{zz} = \frac{E}{(1+P)(1-2P)} \left[ (1-2P)\varepsilon_{zz} - (1+P)\alpha_l x(z) \right], \tag{3.2}$$

where $E$ is the Young's modulus and $P$ is the Poisson's ratio. Combining eqn. (3.2) with the equation of equilibrium for stress, the axial strain can be represented by

$$\varepsilon_{zz} = \left( \frac{1+P}{1-2P} \right) \alpha_l x(z). \tag{3.3}$$

For an exponential variation of composition, the axial strain can be expressed by

$$\varepsilon_{zz} = \left( \frac{1+P}{1-2P} \right) \alpha_l A \left( e^{Cz/z_0} - 1 \right), \tag{3.4}$$

where $z_0$ is the length of the sample. $A$ and $C$ represents the range and slope of the composition along the growth direction, respectively. For the whole range in composition, $A$ = 1. Equation (3.4) can be applied to evaluate the axial strain component at the centerline of a

cylindrically shaped bulk mixed crystal having the gradual variation of composition along the growth direction with axial symmetry. Since 1-D model can not be used to evaluate radial, tangential and shear strain components, it is not usable to understand breakage problem in bulk InGaAs crystals grown by the MCZM method. In order to determine other strain components along with the axial strain component for various compositional profiles in the crystals grown by the two-step MCZM method, axially symmetrical strain model has been discussed in the next section.

## 3.3 Axially Symmetrical Strain Model

The concept of residual strain induced by gradual variation of composition in bulk mixed crystals can be easily realized from Fig. 3.1. For uniform composition, the lattice spacing would not change but would remain constant in the entire crystal. On the other hand, if the composition were to vary in bulk mixed crystals, then the lattice spacing may be compressed or elongated, depending on the

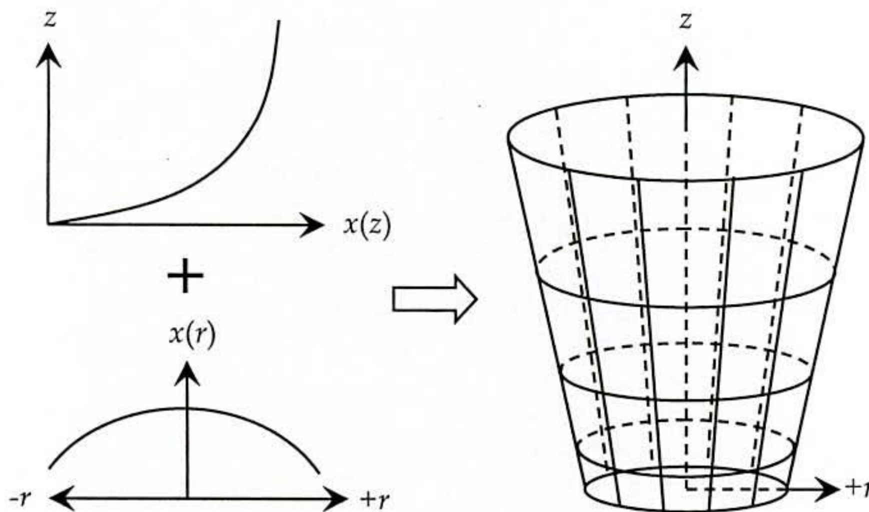


**Fig. 3.1:** Lattice spacing change by the exponential-like compositional variation along the $z$ axis and parabolic compositional variation along the $r$ axis.

compositional profile. The residual strain induced by compositional variation in bulk mixed crystals can be written [32] by

$$\varepsilon[x(r,z)] = \alpha_l[x(r,z)]x(r,z)\,,$$

(3.5)

where $x(r,z)$ is the compositional variation along the $r$ and $z$ axes of the crystal. The rate of change in lattice spacing due to the compositional variation $x(r, z)$ can be expressed [14] by

$$\alpha_l[x(r,z)] = \frac{1}{a[x(r,z)]}\frac{da(x)}{dx}\frac{dx(z)}{dz}x(r)\,, \tag{3.6}$$

where $a[x(r,z)]$ is the compositional dependence of lattice constant. Since the residual strain in bulk mixed crystal is associated with the compositional variation, the state of strain entirely depends on its profile. For instance, if the lattice deformation takes place by the gradient in composition along the growth direction with axial symmetry as shown in Fig. 3.1, the strain components $\varepsilon_{zz}$, $\varepsilon_{rr}$, $\varepsilon_{\theta\theta}$, and $\varepsilon_{rz}$ may exist. The strain phenomena in epilayers are not the same as those in the present bulk mixed crystals. The strain in epilayers is induced due to the abrupt change in lattice spacing between the substrate and epilayer, which can be easily solved by $\varepsilon = a_{sub} - a_{epi}/a_{sub}$ [27-30], where $a_{sub}$ and $a_{epi}$ are the lattice spacing of the substrate and epilayer, respectively. Thus the epilayer strain models cannot be applied to evaluate strain in bulk mixed crystal system.

## 3.4 Analytical Solution of Strains in Cylindrical Co-ordinates

Assuming axial symmetry in isotropic materials, the equations of stress under equilibrium condition [31] reduce to

$$\frac{\partial \sigma_{rr}}{\partial r} + \frac{\partial \tau_{rz}}{\partial z} + \frac{\sigma_{rr} - \sigma_{\theta\theta}}{r} = 0, \tag{3.7}$$

$$\frac{\partial \tau_{rz}}{\partial r} + \frac{\partial \sigma_{zz}}{\partial z} + \frac{\tau_{rz}}{r} = 0, \tag{3.8}$$

where $\sigma_{rr}$, $\sigma_{\theta\theta}$, and $\sigma_{zz}$ are the principal stress components along the radial, tangential, and growth directions, respectively, and $\tau_{rz}$ is the shear stress component. The boundary conditions for the system under investigation are as follows: $0 \le |r| \le r_0$, $0 \le z \le z_0$, where $r_0$ and $z_0$ are the radius and length of the crystal, respectively. The compositional profile $x(r, z)$ becomes zero at $z \to 0$, as a result, the stress components $\sigma_{zz}$, $\sigma_{rr}$, $\sigma_{\theta\theta}$, and $\tau_{rz}$ become zero. Due to the axial symmetry in composition, the stress components $\sigma_{rr} - \sigma_{\theta\theta}$ and $\tau_{rz}$ become zero, at $r \to 0$. By introducing an appropriate stress function: $\phi(r,z)$, the stress components can be expressed in the following forms [31]:

$$\sigma_{zz} = \frac{\partial}{\partial z}\left[(2-P)\nabla^2\phi - \frac{\partial^2 \phi}{\partial z^2}\right], \tag{3.9}$$

$$\sigma_{rr} = \frac{\partial}{\partial z}\left[P\nabla^2\phi - \frac{\partial^2 \phi}{\partial r^2}\right], \tag{3.10}$$

$$\sigma_{\theta\theta} = \frac{\partial}{\partial z}\left[P\nabla^2\phi - \frac{1}{r}\frac{\partial \phi}{\partial r}\right], \tag{3.11}$$

$$\tau_{rz} = \frac{\partial}{\partial r}\left[(1-P)\nabla^2\phi - \frac{\partial^2 \phi}{\partial z^2}\right], \tag{3.12}$$

where $\nabla^2 = \frac{\partial^2}{\partial r^2} + \frac{1}{r}\frac{\partial}{\partial r} + \frac{\partial^2}{\partial z^2}$ and $P$ is the Poisson's ratio. The stress function can be described with polynomials or other forms, which must satisfy both $\nabla^4\phi = 0$ and the boundary conditions in the system under investigation. For our problem, the stress function can be taken

in the form of

$$\phi(r',z') = B(r'^2 + z'^2)^{\frac{1}{2}}, \tag{3.13}$$

where $B$ is a parameter to be determined by the boundary conditions. Here, the normalized variables: $r' = r/r_0$ and $z' = z/z_0$ are used. Substituting Eq. (3.13) into Eqs. (3.9) to (3.12), the stress components can be easily derived as

$$\sigma_{z'z'} = -B\left[(1-2P)(r'^2 + z'^2)^{-\frac{3}{2}} + 3z'^2(r'^2 + z'^2)^{-\frac{5}{2}}\right]z', \tag{3.14}$$

$$\sigma_{r'r'} = B\left[(1-2P)(r'^2 + z'^2)^{-\frac{3}{2}} - 3r'^2(r'^2 + z'^2)^{-\frac{5}{2}}\right]z', \tag{3.15}$$

$$\sigma_{\theta'\theta'} = B\left[(1-2P)(r'^2 + z'^2)^{-\frac{3}{2}}\right]z' \tag{3.16}$$

$$\tau_{r'z'} = -B\left[(1-2P)(r'^2 + z'^2)^{-\frac{3}{2}} + 3z'^2(r'^2 + z'^2)^{-\frac{5}{2}}\right]r'. \tag{3.17}$$

Using boundary conditions, the parameter B was solved [14], which can be expressed as

$$B = \frac{E\alpha_l[x(r',z')]x(r',z')}{(1-2P)(r'^2 + z'^2)^{-1} + 3z'^2(r'^2 + z'^2)^{-2}}. \tag{3.18}$$

By substituting Eq. (3.18) into Eqs. (3.14) to (3.17) and then using the stress-strain relationships [31], the strain components can be obtained [14] as follows:

$$\varepsilon_{z'z'} = -\frac{(1-2P)(1+2P) + 3(z'^2 - r'^2P)(r'^2 + z'^2)^{-1}}{(1-2P)(r'^2 + z'^2)^{\frac{1}{2}} + 3z'^2(r'^2 + z'^2)^{-\frac{1}{2}}}\alpha_l[x(r',z')]x(r',z')z', \tag{3.19}$$

$$\varepsilon_{r'r'} = \frac{(1-2P) - 3(r'^2 - z'^2P)(r'^2 + z'^2)^{-1}}{(1-2P)(r'^2 + z'^2)^{\frac{1}{2}} + 3z'^2(r'^2 + z'^2)^{-\frac{1}{2}}}\alpha_l[x(r',z')]x(r',z')z', \tag{3.20}$$

$$\varepsilon_{\theta'\theta'} = \frac{(1+P)}{(1-2P)(r'^2+z'^2)^{1/2} + 3z'^2(r'^2+z'^2)^{-1/2}} \alpha_l[x(r',z')]x(r',z')z', \qquad (3.21)$$

$$\varepsilon_{r'z'} = -\frac{2(1+P)[(1-2P)+3z'^2(r'^2+z'^2)^{-1}]}{(1-2P)(r'^2+z'^2)^{1/2} + 3z'^2(r'^2+z'^2)^{-1/2}} \alpha_l[x(r',z')]x(r',z')r', \qquad (3.22)$$

$$\varepsilon_{r'r'} - \varepsilon_{\theta'\theta'} = -\frac{3[P+(r'^2-z'^2P)(r'^2+z'^2)^{-1}]}{(1-2P)(r'^2+z'^2)^{1/2} + 3z'^2(r'^2+z'^2)^{-1/2}} \alpha_l[x(r',z')]x(r',z')z' \quad (3.23)$$

Under the influence of the above strain components, the lattice spacing will be deformed along both the $z$ and $r$ axes of the crystal. Here, the effective strain component $\varepsilon_{r'r'} - \varepsilon_{\theta'\theta'}$ is introduced to understand the resultant deformation of lattice constant along the $r$ axis. If the compositional profile of the crystal is known, the quantitative amount of strain can be determined using equations (3.19) to (3.23).

In order to apply the model for various compositional profiles, the composition function may be generally written in a polynomial form:

$$x(r',z') = A\left(1 \pm \sum_{n=0}^{N} C_{2n} z'^{2n} r'^{2n}\right)\left(\sum_{k=0}^{K} D_k z'^k\right), \qquad (3.24)$$

where $A$ is a constant, by which the range of composition along the growth direction can be adjusted. The shape of compositional profile along the radial and growth directions can be adjusted by the constants $C_{2n}$ and $D_k$, respectively.

## 3.5 Strain Distribution in Bulk $In_xGa_{1-x}As$ Mixed Crystals for Various Compositional Profiles

Using equations (3.19-3.23) the quantitative amount of strains and their distributions are investigated in bulk $In_xGa_{1-x}As$ mixed crystals for the combination of different typical compositional profiles

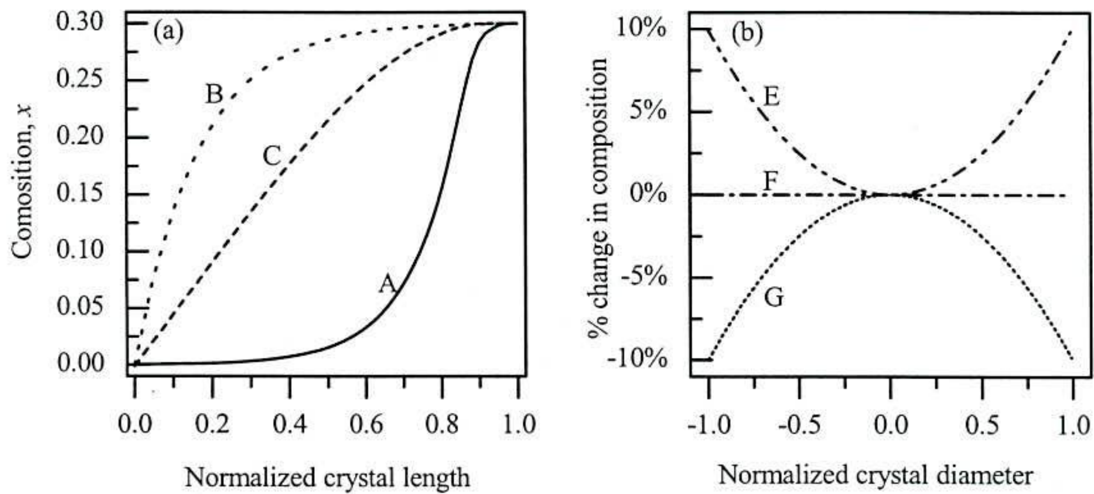


**Fig 3.2:** Typical compositional profiles a) along the growth direction, b) along the radial direction of the crystal. Actual profile may be any combination of the profiles A, B, or C with the profiles E, F, or G.

shown in Fig. 3.2(a) and 3.2(b). The variations of composition along the growth direction of the crystal are defined by three profiles: i) exponential growth like-profile 'A', ii) exponential associate like-profile 'B', and iii) linear like-profile 'C' as indicated in Fig 3.2(a). Since it is expected to investigate strain distribution in bulk InGaAs mixed crystal for simultaneous variation of composition along the growth and radial directions, the radial profiles are defined by upward parabolic like-profile 'E', flat like-profile 'F', and downward parabolic like-profile 'G' as seen in Fig. 3.2(b). For the simultaneous variation of composition along the growth and radial directions of the crystal, complete profiles AE, AF, and AG, BE, BF, and BG, and CE, CF, and CG can be understood with the combination of the profiles A, B, and C with those of the E, F, and G. It is to be mentioned here that the compositional profile in InGaAs crystal grown by the MCZM method is increased gradually at the initial stage by controlling the temperature profile. The resulting compositional profile obtained from this growth method is also shown in Fig. 1.2, which is similar to the typical profile

A as shown in Fig 3.2(a). Although radial profile was not found symmetrical in bulk InGaAs crystals grown by the MCZM method (Fig.

**Table 3.1:** Physical constants in GaAs and InAs crystals [33].

| | GaAs | InAs |
|---|---|---|
| Lattice constant α [A°] | 5.6533 | 6.0584 |
| Poisson's ratio P | 0.37 | 0.43 |

2.5), it is expected to be symmetrical in most of the growth processes depending on the radial temperature profile in the furnace. Since our main target is to obtain compositional homogeneity over the whole region of the crystal, compositional symmetry along the radial direction can be considered. In the present analysis, the range of composition is assumed to be $0 \le x \le 0.3$ along the growth direction of the crystal while ±10% variation of composition is assumed in the radial direction. In order to evaluate the quantitative amount of strains physical constants listed in Table 3.1 for the GaAs and InAs materials are used in the present calculation.

### 3.5.1 Strain Distribution for the Profiles AF, BF and CF

Using an axially symmetrical strain model axial strain ($\varepsilon_{z'z'}$), radial strain ($\varepsilon_{r'r'}$), tangential strain ($\varepsilon_{\theta'\theta'}$) and shear strain ($\varepsilon_{r'z'}$) components corresponding to the compositional profiles AF, BF and CF are evaluated. Figures 3.3(a)–3.3(o) show a comparison of strain distributions evaluated for the compositional profiles AF, BF and CF at the centre ($r' = 0$), between the center and periphery ($r' = 0.5$) and at the periphery ($r' = 1$) of a cylindrical-shaped crystal as a function of normalized crystal length where the normalized length is taken from

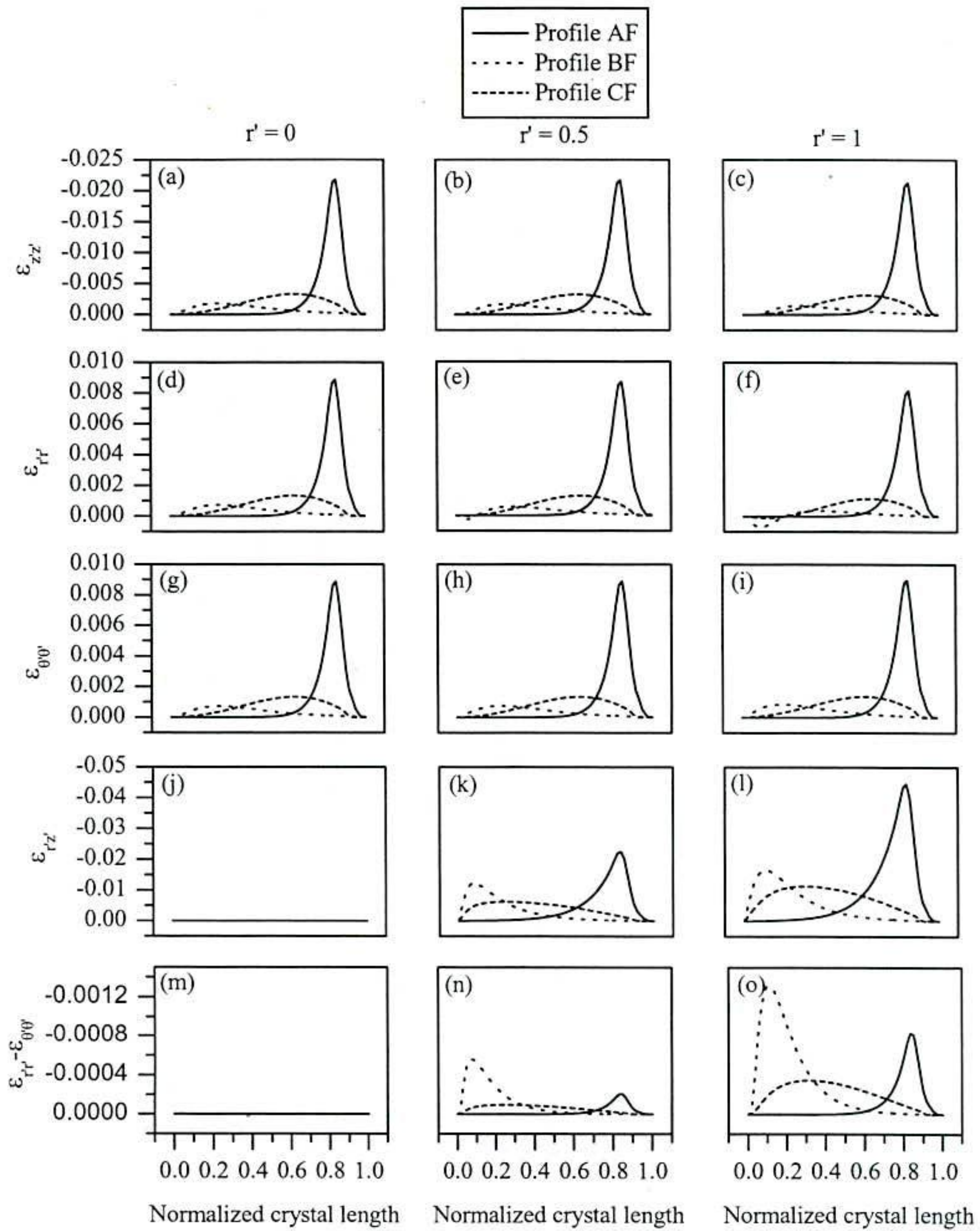


**Fig. 3.3:** Strain distributions along the length of a cylindrical-shaped bulk InGaAs crystal for the compositional profiles AF, BF and CF at three different radial positions [centre ($r' = 0$), between centre and periphery ($r' = 0.5$) and periphery ($r' = 1$)].

the seed end. The strain distributions obtained for the compositional profiles AF, BF and CF are indicated by the solid, doted and dashed

**Table 3.2:** Maximum strain values at the three different radial positions ($r'=0$, $r'=0.5$, and $r'=1$) for the compositional profiles AF, BF, and CF.

| Composi- -tional profiles | Strain component | Normalized crystal length | Maximum strain | | |
|---|---|---|---|---|---|
| | | | $r'=0$ | $r'=0.5$ | $r'=1$ |
| AF | $\varepsilon_{z'z'}$ | 0.83 | -0.0218 | -0.02167 | -0.02128 |
| BF | | 0.25 | -0.00179 | -0.00167 | -0.00142 |
| CF | | 0.63 | -0.00329 | -0.00325 | -0.00314 |
| AF | $\varepsilon_{r'r'}$ | 0.83 | 0.00886 | 0.00868 | 0.00816 |
| BF | | 0.25 | 0.000726 | 0.000587 | 0.000372 |
| CF | | 0.63 | 0.00134 | 0.00129 | 0.00116 |
| AF | $\varepsilon_{\theta'\theta'}$ | 0.83 | 0.00886 | 0.00889 | 0.00898 |
| BF | | 0.25 | 0.000726 | 0.000757 | 0.000845 |
| CF | | 0.63 | 0.00134 | 0.00134 | 0.00137 |
| AF | $\varepsilon_{r'z'}$ | 0.83 | 0 | -0.02257 | -0.04461 |
| BF | | 0.1 | 0 | -0.01227 | -0.01655 |
| CF | | 0.31 | 0 | -0.00626 | -0.01141 |
| AF | $\varepsilon_{r'r'}-\varepsilon_{\theta'\theta'}$ | 0.83 | 0 | -0.0002 | -0.00083 |
| BF | | 0.1 | 0 | -0.00056 | -0.00132 |
| CF | | 0.31 | 0 | -0.00009 | -0.00034 |

lines, respectively. It is found in Fig. 3.3 that the $\varepsilon_{z'z'}$, $\varepsilon_{r'r'}$ and $\varepsilon_{\theta'\theta'}$ strain values are maximum near the seed-end of the crystal for the profile BF. The same strain values are found to be maximum near the middle and at the end of the first step growth process, respectively, for the profiles CF and AF. The maximum amount of strains evaluated in various radial positions of the crystal corresponding to the profiles AF, BF and CF are summarized in Table 3.2. The shear strain component $\varepsilon_{r'z'}$ is very important for understanding crystal breakage issue in bulk mixed crystal having compositional gradient. It is found in Fig. 3.3(j) that the $\varepsilon_{r'z'}$ strain component is zero along the growth axis of the crystal due to the axial symmetry in composition. However, apart from

the growth axis, it increases with increasing the composition for the profile AF and it reaches to its maximum value of -0.04461 at $r' = 1$ near the normalized crystal length of 0.83 and then it is reduced drastically to zero when the lattice spacing becomes constant due to compositional homogeneity. For the profile BF, $\varepsilon_{r'z'}$ reaches to its maximum value of -0.01655 at the normalized crystal length of 0.1 at $r' = 1$. It is then gradually reduced to zero at the end of the first step growth of the crystal. For the profile CF, $\varepsilon_{r'z'}$ reaches to its maximum value of -0.01141 at the normalized crystal length of 0.31. It is then gradually reduced to zero at the end of the first step growth due to the compositional homogeneity. For this profile, the maximum shear strain is found to be lower than that of the other two profiles AF and BF. From Figs. 3.3(m)-3.3(o) resultant radial strain $\varepsilon_{r'r'} - \varepsilon_{\theta'\theta'}$ is found to be zero at the centre and then it is increased as we approach towards the periphery for all compositional profiles. The results shown in Table 3.2 demonstrate that the values of strains induced at different positions of the crystal are highly sensitive to the shape of the compositional profiles.

It is mentioned here that the compositional profile AF is similar to the profile currently being used in the MCZM growth process. According to the behavior of the profile AF, the rate of change in lattice spacing is drastic at the end of the first step growth in the two-step MCZM growth process. Once the composition becomes homogeneous, the rate of change in lattice spacing also becomes zero. As a result, this region of the crystal shows drastic change in strain values for the profile AF as seen in Fig. 3.3. This drastic change in strain magnitude helps us to understand the crystal breakage mechanism in the two-step MCZM growth technique. Since rate of change in lattice spacing for the profiles BF and CF is not like the profile AF, the strain accumulation characteristics in these profiles are quite different. Due to these facts, lower strain values are found for the profiles BF and CF

than that of the profile AF as clearly demonstrated in Fig. 3.3.

### 3.5.2 Strain Distribution for the Profiles AE, BE and CE

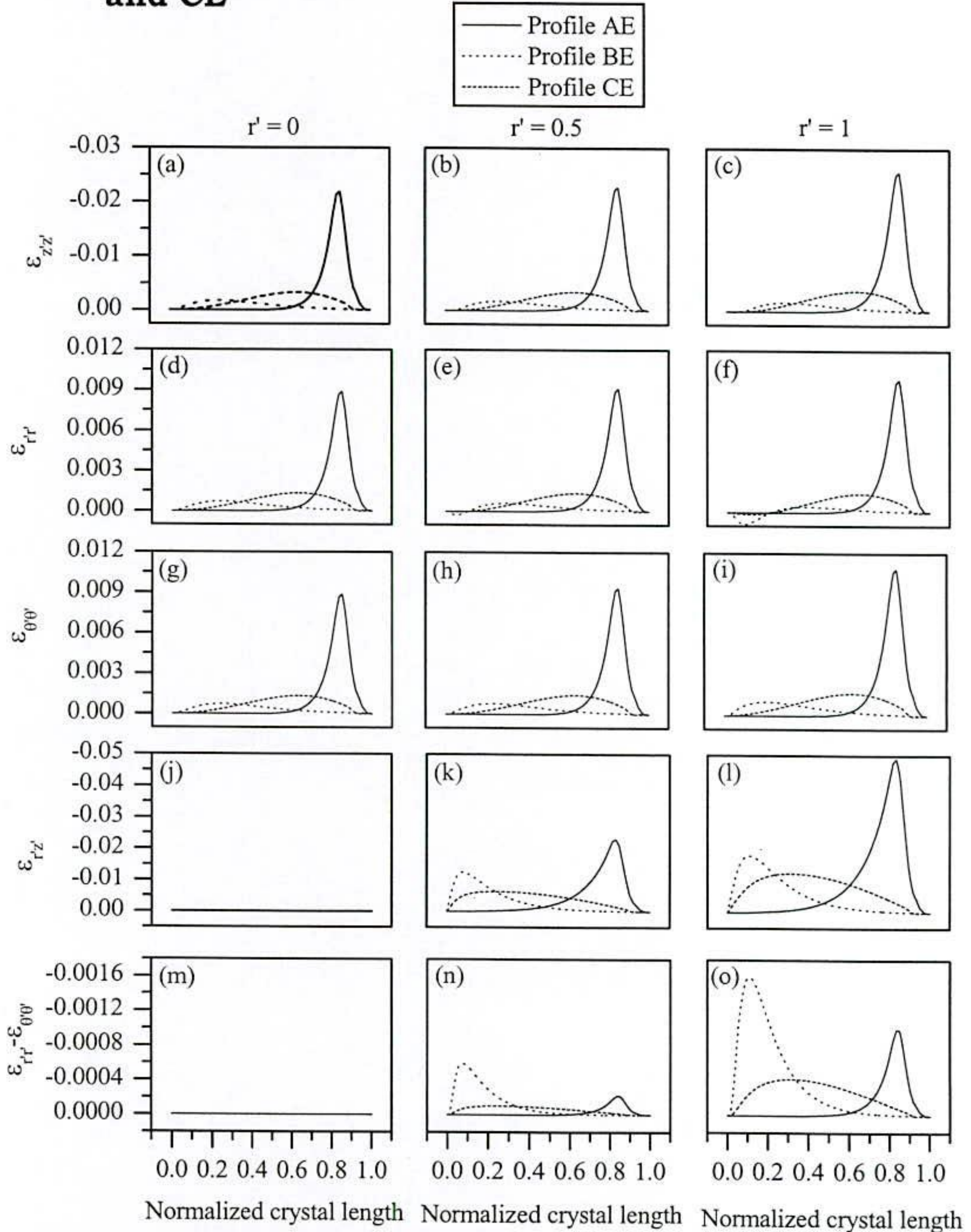


**Fig. 3.4:** Strain distributions along the length of a cylindrical-shaped bulk InGaAs crystal for the compositional profiles AE, BE and CE at three different radial positions [centre ($r'=0$), between centre and periphery ($r'=0.5$) and periphery ($r'=1$)].

Axially symmetrical strain model is further used to evaluate $\varepsilon_{z'z'}$, $\varepsilon_{r'r'}$, $\varepsilon_{\theta'\theta'}$ and $\varepsilon_{r'z'}$ for the profiles AE, BE and CE. Figures 3.4(a)–3.4(o) show a comparison of strain distributions evaluated for the compositional profiles AE, BE and CE with the same conditions as seen in Figs. 3.4(a)–3.4(o). The strain distributions obtained for the compositional profiles AE, BE and CE are also indicated by the solid, doted and dashed lines, respectively. It is observed from Figs. 3.4(a)–3.4(o) that the strain distributions for the profiles AE, BE and CE are almost similar with those of the profiles AF, BF and CF. However, the amount of strains are found to be different along the radial direction for the

**Table 3.3:** Maximum strain values at the three different radial positions ($r'=0$, $r'=0.5$, and $r'=1$) for the compositional profiles AE, BE, and CE.

| Composi-tional profiles | Strain component | Normalized crystal length | Maximum strain | | |
|---|---|---|---|---|---|
| | | | $r'=0$ | $r'=0.5$ | $r'=1$ |
| AE | $\varepsilon_{z'z'}$ | 0.83 | -0.0218 | -0.02276 | -0.02569 |
| BE | | 0.25 | -0.00179 | -0.00175 | -0.00171 |
| CE | | 0.63 | -0.00329 | -0.00341 | -0.0038 |
| AE | $\varepsilon_{r'r'}$ | 0.83 | 0.00886 | 0.00912 | 0.00988 |
| BE | | 0.25 | 0.000726 | 0.000617 | 0.00045 |
| CE | | 0.63 | 0.00134 | 0.00135 | 0.0014 |
| AE | $\varepsilon_{\theta'\theta'}$ | 0.83 | 0.00886 | 0.00934 | 0.01087 |
| BE | | 0.25 | 0.000726 | 0.000796 | 0.00102 |
| CE | | 0.63 | 0.00134 | 0.00141 | 0.00166 |
| AE | $\varepsilon_{r'z'}$ | 0.83 | 0 | -0.02313 | -0.04904 |
| BE | | 0.1 | 0 | -0.01258 | -0.0182 |
| CE | | 0.31 | 0 | -0.00642 | -0.01255 |
| AE | $\varepsilon_{r'r'}-\varepsilon_{\theta'\theta'}$ | 0.83 | 0 | -0.00022 | -0.0001 |
| BE | | 0.1 | 0 | -0.000591 | -0.0016 |
| CE | | 0.31 | 0 | -0.000102 | -0.00042 |

present profiles than those of the previous profiles. The maximum amount of strains evaluated at $r' = 0$, $r' = 0.5$ and $r' = 1$ corresponding to the profiles AE, BE and CE are listed in Table 3.3. As shown in Table 3.3 the shear strain component $\varepsilon_{r'z'}$ is found to be zero along the growth axis of the crystal due to the axial symmetry in composition. However, apart from the growth axis, it increases with increasing the composition for the profile AE and it reaches to its maximum value of -0.04904 at $r' = 1$ near the normalized crystal length 0.83. It then falls to zero as the lattice spacing becomes constant at the end of the first step growth. For the profile BE, $\varepsilon_{r'z'}$ reaches to its maximum value of -0.0182 at $r' = 1$ near the normalized crystal length 0.1. It then gradually falls to zero at the end of the first step growth. In case of the profile CE, $\varepsilon_{r'z'}$ reaches to its maximum value of -0.01255 at the normalized crystal length 0.31 which is the smallest compared to those evaluated for the profiles AE and CE. Maximum values of resultant radial strains are found to be -0.0001, -0.0016 and -0.00042 near the homogeneous composition region, the seed end and the normalized crystal length 0.31, respectively, for the profiles AE, BE and CE. This strain value is found to be increased along the radial direction with crystal length for all the profiles. Therefore, the strain distributions and their magnitudes are found to be highly dependent on the shape compositional profiles.

### 3.5.3 Strain Distribution for the Profiles AG, BG and CG

Strain distributions for $\varepsilon_{z'z'}$, $\varepsilon_{r'r'}$, $\varepsilon_{\theta'\theta'}$ and $\varepsilon_{r'z'}$ strain components are also evaluated using the same procedure as discussed before corresponding to the profiles AG, BG and CG as shown in figures 3.5(a)–3.5(o). These strain values are evaluated at

different radial positions as a function of normalized crystal length which is indicated

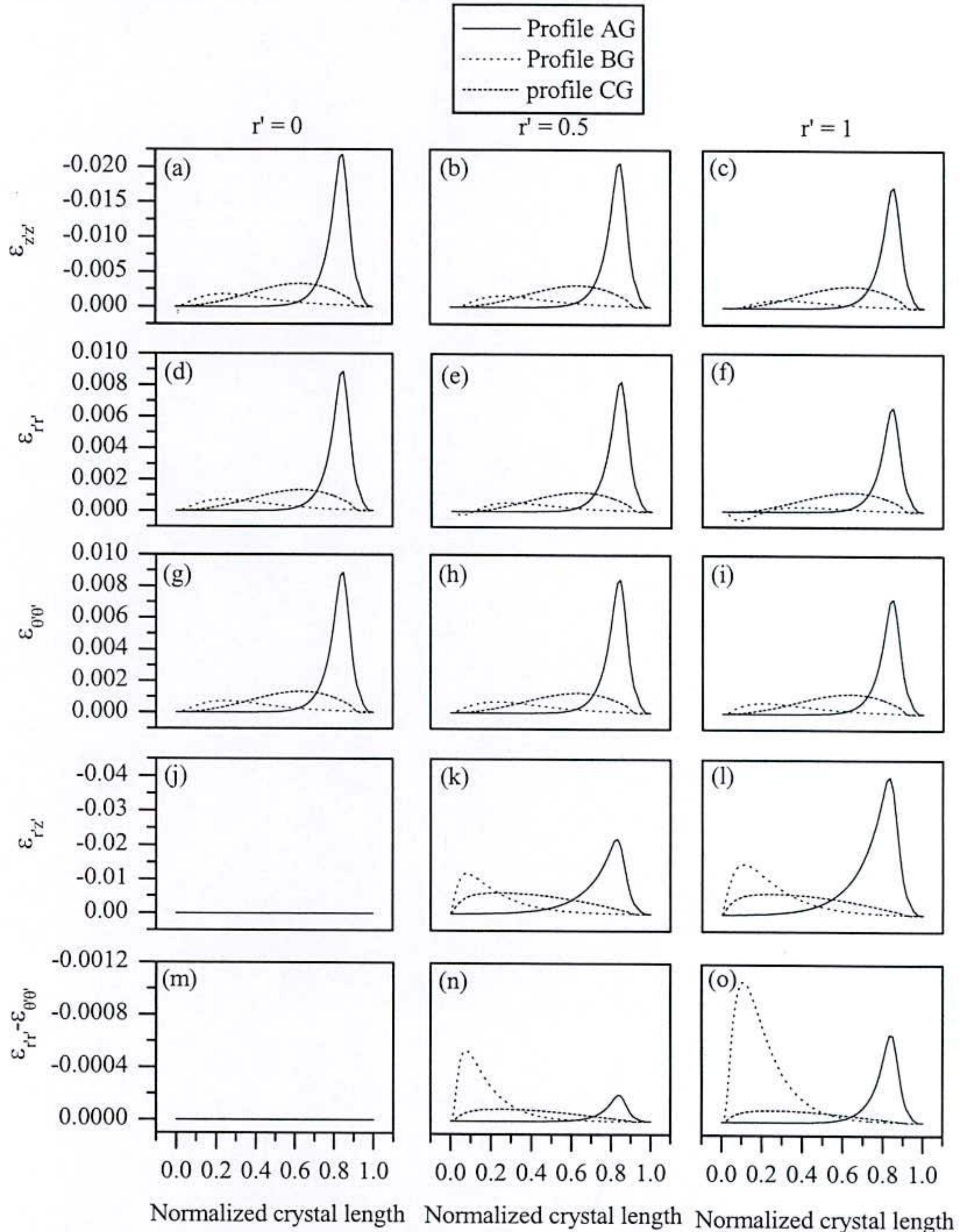


**Fig. 3.5:** Strain distributions along the length of a cylindrical-shaped bulk InGaAs crystal for the compositional profiles AG, BG and CG at three different radial positions [centre ($r' = 0$), between centre and periphery ($r' = 0.5$) and periphery ($r' = 1$)].

**Table 3.4:** Maximum strain values at the three different radial positions ($r' = 0$, $r' = 0.5$, and $r' = 1$) for the compositional profiles AG, BG, and CG.

| Composi- -tional profiles | Strain componet | Normalized crystal length | Normalized radial distance | | |
|---|---|---|---|---|---|
| | | | $r' = 0$ | $r' = 0.5$ | $r' = 1$ |
| AG | $\varepsilon_{z'z'}$ | 0.83 | -0.0218 | -0.02061 | -0.01727 |
| BG | | 0.25 | -0.00179 | -0.00159 | -0.00115 |
| CG | | 0.63 | -0.00329 | -0.00309 | -0.00331 |
| AG | $\varepsilon_{r'r'}$ | 0.83 | 0.00886 | 0.00825 | 0.00661 |
| BG | | 0.25 | 0.000726 | 0.000558 | 0.000301 |
| CG | | 0.63 | 0.00134 | 0.00123 | 0.00121 |
| AG | $\varepsilon_{\theta'\theta'}$ | 0.83 | 0.00886 | 0.00845 | 0.00727 |
| BG | | 0.25 | 0.000726 | 0.00072 | 0.000684 |
| CG | | 0.63 | 0.00134 | 0.00128 | 0.00125 |
| AG | $\varepsilon_{r'z'}$ | 0.83 | 0 | -0.02201 | -0.04017 |
| BG | | 0.1 | 0 | -0.01197 | -0.0149 |
| CG | | 0.31 | 0 | -0.00611 | -0.0611 |
| AG | $\varepsilon_{r'r'} - \varepsilon_{\theta'\theta'}$ | 0.83 | 0 | -0.0002 | -0.00061 |
| BG | | 0.1 | 0 | -0.00053 | -0.00107 |
| CG | | 0.31 | 0 | -0.00009 | -0.00009 |

in Fig. 3.5. Similar to the previous figures, the solid, doted and dashed lines in Fig. 3.5 correspond to the profiles AG, BG and CG, respectively. The maximum amount of strains for various radial positions and crystal lengths are listed in Table 3.4 corresponding to the profiles AG, BG and CG. The strain magnitudes, $\varepsilon_{z'z'}$, $\varepsilon_{r'r'}$ and $\varepsilon_{\theta'\theta'}$ are found to be the lowest at the periphery of the crystal and then increase gradually as moving from the periphery to the centre of the crystal. This tendency is different than those of the profiles discussed before. Alike of the previous profiles the strain component $\varepsilon_{r'z'}$ is found to be zero at the centre for the present profiles. This is resulted from the compositional symmetry along the radial direction. The

highest values of shear strain are accumulated near the seed-end and at the end of the first step growth for the profiles BG and AG, respectively. On the other hand its distribution is found to be almost uniform up to the 60% crystal length for the profile CG. It is also found that the value of shear strain changes drastically at the end of the first step growth process for the profile AG. In contrast, the shear strain is changed gradually at the end of the first step growth process for the profiles BG and CG. Furthermore, the distributions of the resultant radial strain are found to be similar to the shear strain for all the profiles.

## 3.6 Summary

In this chapter, axially symmetrical strain model has been applied to investigate strain distributions in bulk InGaAs crystals for typical compositional profiles, which can be used in MCZM growth process. Strain components for nine different compositional profiles have been analyzed among which the profiles AF, AE and AG are similar to the profile which is currently being used in the MCZM growth technique. It is found from the distributions that the strain components are dependent on the compositional variations and shape of the profiles. In the profiles AF, AE and AG, the strain values are found to be increased gradually near the seed-end due to the gradual change in composition. However, these profiles show a drastic increase in the strain near the homogeneous composition region of the crystal where the first step growth process ends. This is due to the drastic change in lattice constant for these profiles. The maximum values of strains are obtained at the 83% crystal length where the rate of change of composition is the highest. The strain values are then suddenly reduced to zero as the composition becomes constant. This drastic change of strains is very much important to elucidate the breakage issue in the InGaAs crystal grown by the MCZM method. In

the profiles BF, BE and BG, strain values are increased considerably at the seed-end of the crystal and then these values are gradually reduced to zero while approaching towards the homogeneous composition region. On the other hand, profiles CF, CE and CG show lower values of strain compared to the other profiles. In this chapter, strain distributions have been investigated by the line diagram at three different radial positions of the crystal. To understand the spatial variation of strain in the entire region of the crystal, two dimensional mapping of strain has been developed for various compositional profiles, which is presented in the next chapter.

Chapter 4

# Two-dimensional Mapping of Composition and Strain

## 4.1 Introduction

In this chapter, two-dimensional mapping of composition and strain has been developed to investigate the spatial variation of strain under various compositional profiles in bulk InGaAs crystals.

Residual strain induced by compositional variation in bulk mixed crystals is one of the main causes of crystal breakage in MCZM growth technique, which is confirmed in chapter two with the combination of Raman scattering, photoluminescence and energy dispersive X-ray measurements. In the preceding chapter, strain distributions in bulk InGaAs crystal have been investigated for various compositional profiles and then compared them by the line diagram. It is found that the quantitative amount of strain in bulk InGaAs crystal is highly sensitive to the compositional profile and its range. Since the line diagram is not suitable to understand the spatial variation of strain, a two-dimensional mapping of strain and composition is developed here which will enable us to explain the strain distributions precisely in the entire region of the crystal. In this mapping system, color maps are constructed with a spatial resolution of 50 μm corresponding to the strain values evaluated along the radial and growth directions of the crystal. The mapping of strain, plotted under various compositional profiles, would be helpful to explain the relationship between the crystal breakage mechanisms and the shape

of the compositional profile. In this chapter, two-dimensional color maps constructed for different strain components have been presented corresponding to the typical compositional profiles AE, BE, CE, AG, BG, CG, AF, BF and CF discussed in chapter 3.

## 4.2 Two-dimensional Composition and Strain Maps

### 4.2.1 Maps for the profiles AE, BE and CE

#### 4.2.1.1 Composition Maps

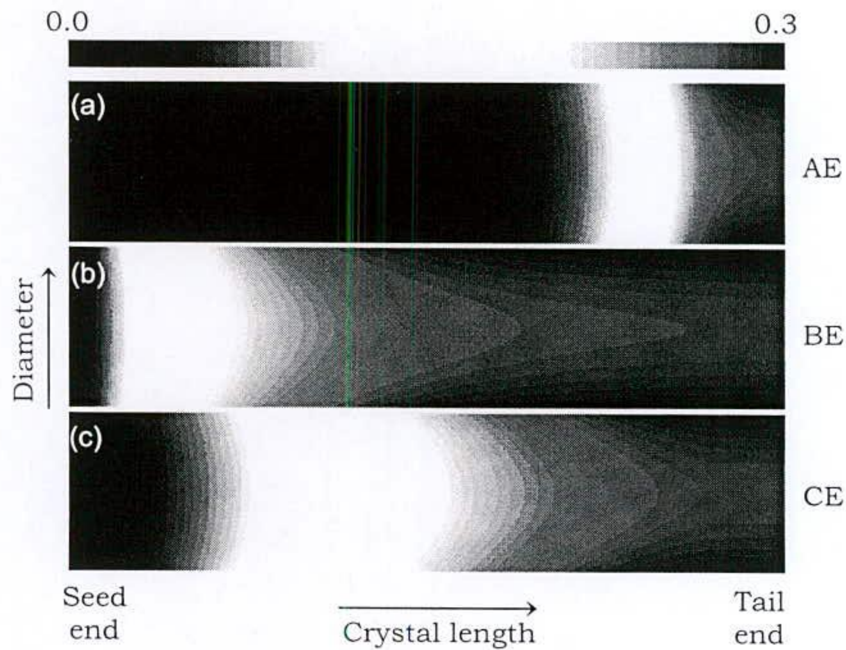


**Fig. 4.1:** Composition maps for the profiles AE, BE and CE.

### 4.2.1.2 Axial Strain Maps

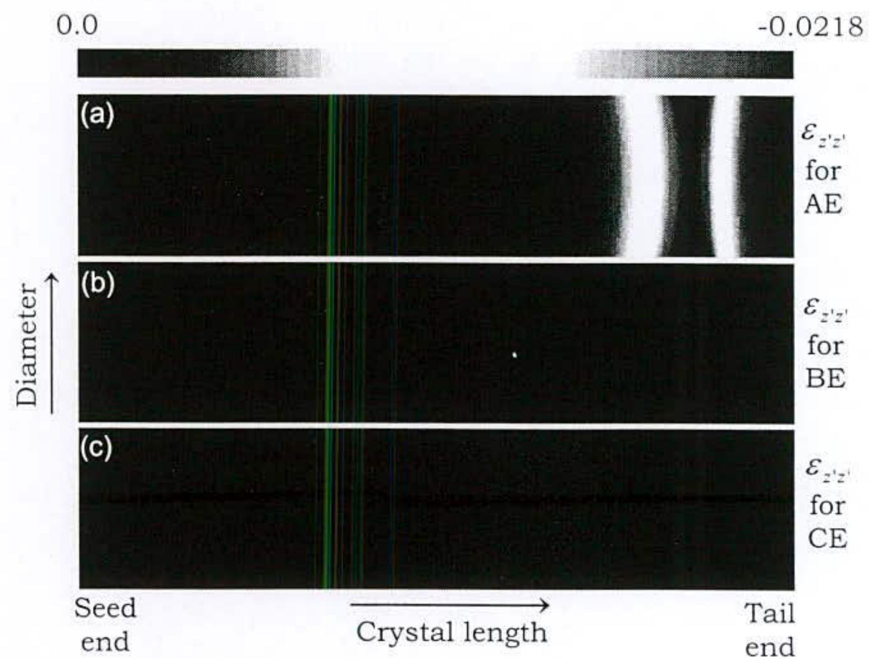


**Fig. 4.2:** Axial strain maps for the profiles AE, BE and CE.

### 4.2.1.3 Radial Strain Maps

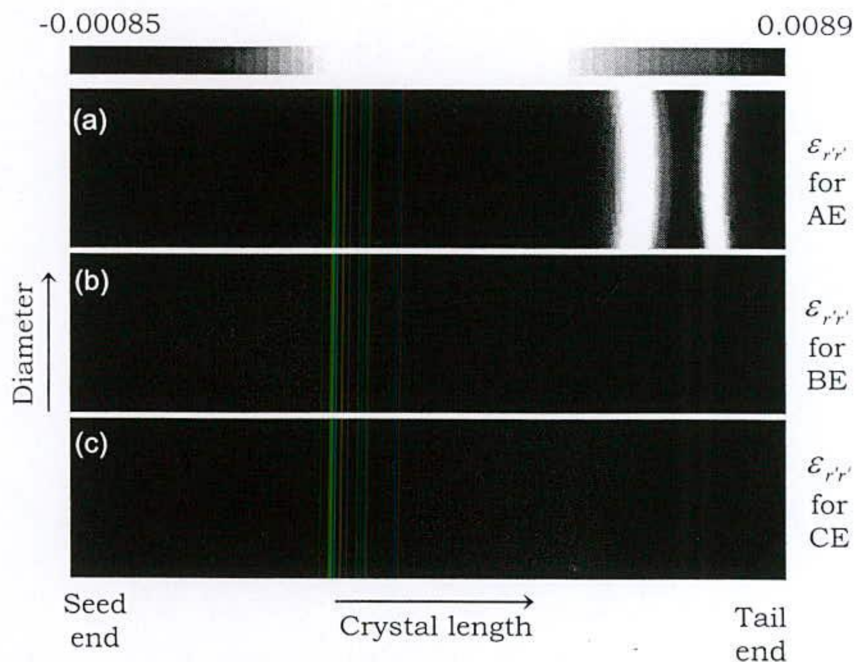


**Fig. 4.3:** Radial strain maps for the profiles AE, BE and CE.

#### 4.2.1.4 Tangential Strain Maps

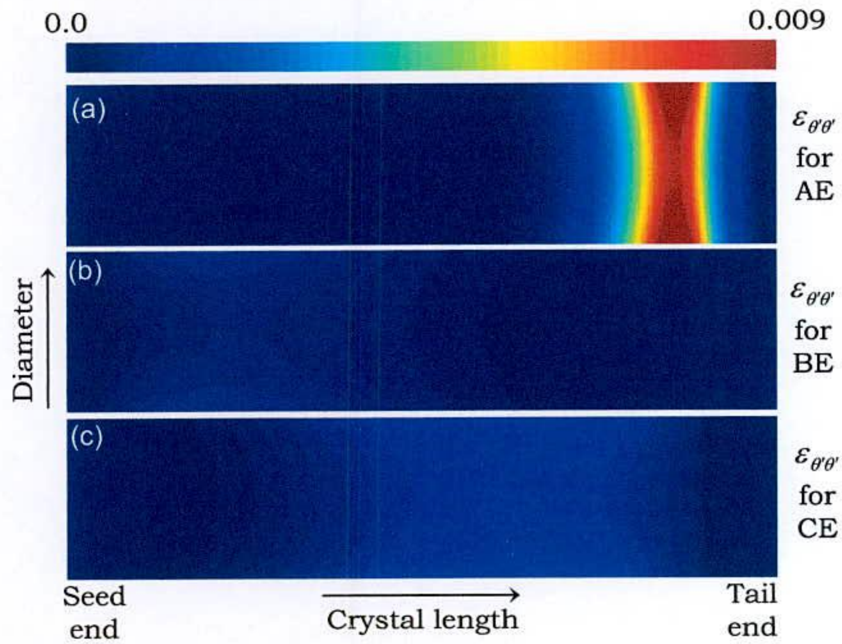


**Fig. 4.4:** Tangential strain maps for the profiles AE, BE and CE.

#### 4.2.1.5 Shear Strain Maps

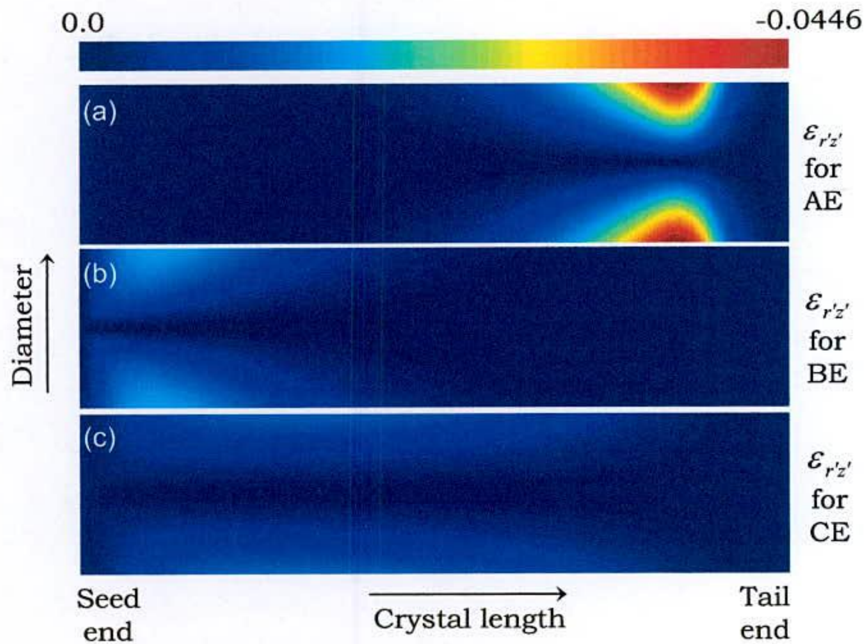


**Fig. 4.5:** Shear strain maps for the profiles AE, BE and CE

#### 4.2.1.6 Resultant Radial Strain Maps

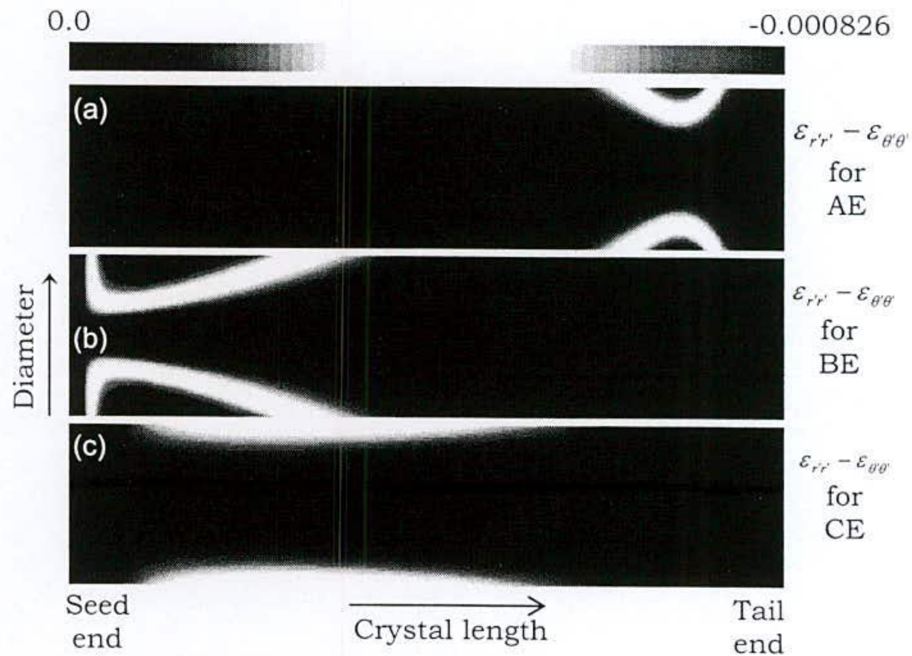


**Fig. 4.6:** Resultant radial strain maps for the profiles AE, BE and CE.

Figures 4.1(a)-4.1(c) show the composition maps for the profiles AE, BE and CE, respectively. In case of the profile AE, the composition is increased gradually near the seed-end and drastically near the homogeneous composition region as indicated by the change in colors in Fig. 4.1(a). The values of composition corresponding to each color can easily be understood form the color scale as shown at the top of Fig. 4.1. However, in case of the profile BE, the composition is increased drastically near the seed-end and gradually near the homogeneous composition region of the crystal as seen in Fig. 4.1(b). On the other hand, the composition in case of the profile CE is increased almost linearly up to a certain value and then it becomes gradually uniform when the composition reaches to the value of 0.3 as shown in Fig. 4.1 (c). In all the three cases, the variation of composition at the periphery is 10% higher than that of the centre

along the radial direction as clearly indicated by colors in the composition maps.

Axial ($\varepsilon_{z'z'}$), radial ($\varepsilon_{r'r'}$) and tangential ($\varepsilon_{\theta'\theta'}$) strain maps corresponding to the profiles AE, BE and CE are shown in Figs 4.2, 4.3 and 4.4, respectively. The strain maps obtained for a particular strain component for various compositional profiles are plotted in normalized scale to compare the quantitative amount of strains and their distributions. For the profile AE, the values of $\varepsilon_{z'z'}$, $\varepsilon_{r'r'}$ and $\varepsilon_{\theta'\theta'}$ strains are found to be maximum at the periphery near the homogeneous composition region of the crystal. On the other hand, the values of these strain components are found to be maximum near the seed-end for the profile BE, although their amount is found to be maximum near the 60% length of the crystal for the profile CE. Such behavior of strain distributions resulted from the rate of change in composition in the profiles AE, BE and CE. A comparison among the color maps plotted for the strain components $\varepsilon_{z'z'}$, $\varepsilon_{r'r'}$ and $\varepsilon_{\theta'\theta'}$ reveals that these strain values are much higher near the end of the first step growth for the profile AE than those for the profiles BE and CE. Further, these strain values are found to be higher at the periphery than at the centre of the crystal along the radial direction. This is due to the parabolic increment of composition from the centre to the periphery along the radial direction of the crystal.

Figure 4.5 shows a comparison among the shear strain maps, which are constructed for the profiles AE, BE and CE. It is well known that the shear strain component plays the key role for making cracks in any material. Therefore, the maps of shear strain are more interesting and important in investigating and understanding the breakage issue in the bulk InGaAs crystals grown by the two-step MCZM method. For all the profiles, it is found that the shear strain zero along the growth axis of the crystal due to the axial symmetry in composition. Apart from the centerline, it is found to be increased

along the radial direction. For the profile AE, $\varepsilon_{r'z'}$ is accumulated to its maximum value near the periphery of the crystal where the composition starts to become homogeneous at the end of the first step growth. It is then drastically reduced to zero when the composition becomes homogeneous. It is noticed here that the compositional profile used at the first step growth of the MCZM growth process is similar to the profile AE. Thus, the crystal breakage issue in the MCZM crystal may be associated with this drastic change in shear strain near the homogeneous composition region of the crystal.

In order to solve the breakage issue in InGaAs bulk mixed crystals, this strain value must be lower, especially near the region of homogeneous composition where the first step growth is ended. Maps of $\varepsilon_{r'z'}$ for the profiles BE and CE, show lower value of strain near the region of homogeneous composition. For the profile BE, it is maximum at the periphery near the seed-end and then gradually reduces to zero with increasing the crystal length. On the other hand, for the profile CE $\varepsilon_{r'z'}$ is found to be lower at the seed-end. Apart form the seed-end, it starts increasing gradually along the radial direction for a certain crystal length and then starts to reduce gradually up to the crystal length where the composition tends to homogeneous. When the composition becomes uniform, it is then reduced to zero as shown in Fig. 4.5(c). Further, it is found from a comparison among Figs. 4.5(a)-(c) that the amount of $\varepsilon_{r'z'}$ is lower for the profile CE than the profiles AE and BE.

Figure 4.6 shows resultant radial strain maps for the profiles AE, BE and CE. This strain component helps us to understand lattice deformation along the radial direction. From Fig. 4.6(a), it is found that, $\varepsilon_{r'r'} - \varepsilon_{\theta'\theta'}$ is the highest for the profile AE at the periphery near the homogeneous composition region of the crystal. Further, the highest value of $\varepsilon_{r'r'} - \varepsilon_{\theta'\theta'}$ for the profile BE is found at the periphery near the seed-end of the crystal. For the profile CE, it is found to be

almost uniform along the growth axis, although there is a small change in $\varepsilon_{r'r'} - \varepsilon_{\theta'\theta'}$ is found along the radial direction for a certain crystal length away from the seed-end. Among the three profiles, the smallest value of $\varepsilon_{r'r'} - \varepsilon_{\theta'\theta'}$ is obtained for the profile CE, which demonstrates that the lattice deformation is smaller along the radial direction for the profile CE.

## 4.2.2 Map for the Profiles AG, BG and CG

### 4.2.2.1 Composition Maps

Figure 4.7(a)-4.7(c) show the composition maps for the profiles AG, BG and CG, respectively, where the variation of composition is the same along the crystal growth direction as shown in the previous profiles. However, instead of upward parabolic variation a downward parabolic variation of composition is considered along the radial direction where the composition is decreased by 10% from the centre to the periphery of the crystal.

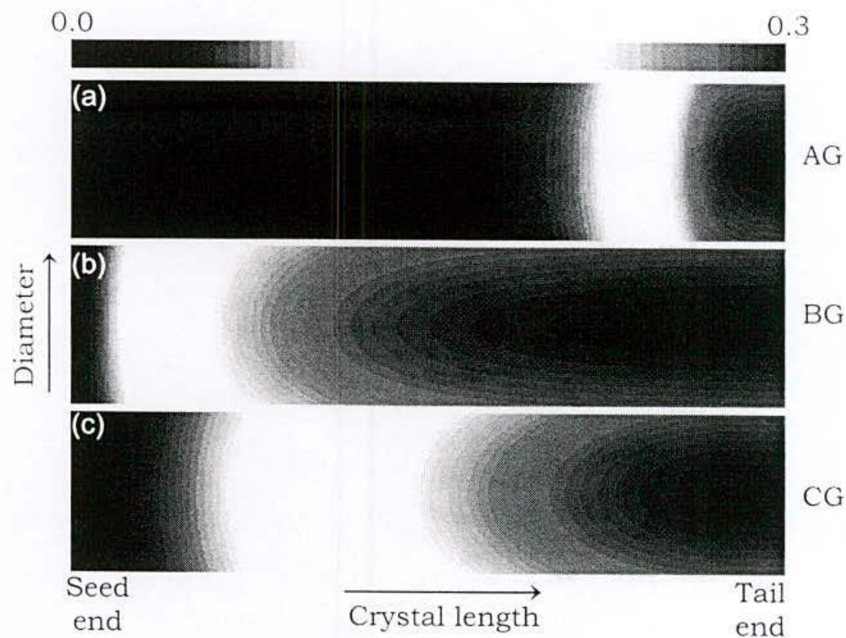


**Fig. 4.7:** Composition maps for the profiles AG, BG and CG.

#### 4.2.2.2 Axial Strain Maps

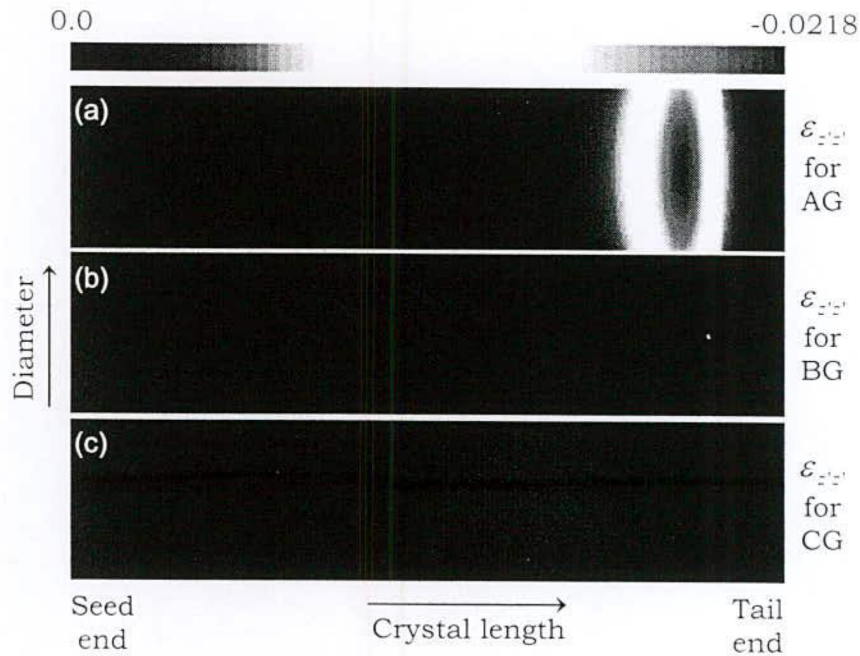


**Fig. 4.8:** Axial strain maps for the profiles AG, BG and CG.

#### 4.2.2.3 Radial Strain Maps

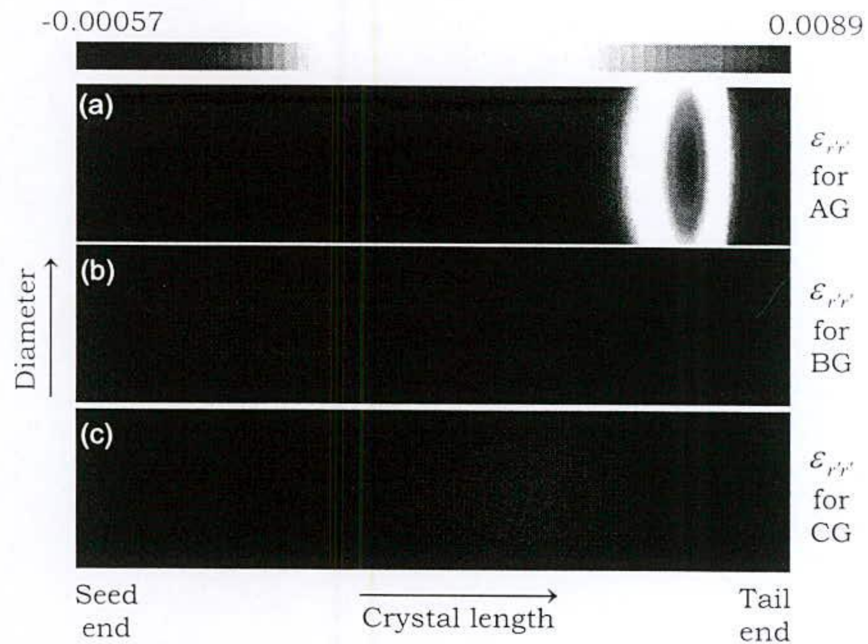


**Fig. 4.9:** Radial strain maps for the profiles AG, BG and CG.

#### 4.2.2.4 Tangential Strain Maps

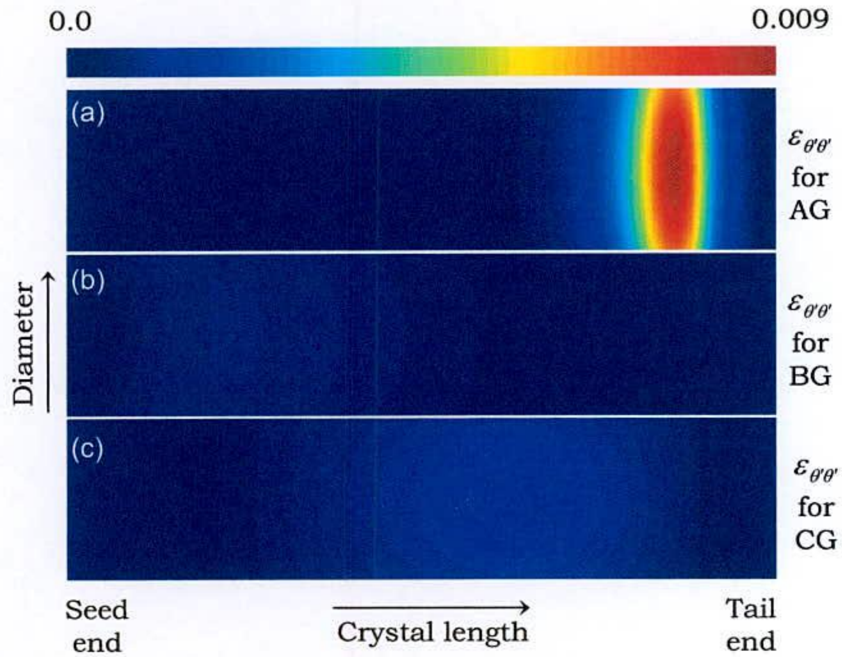


**Fig. 4.10:** Tangential strain maps for the profiles AG, BG and CG.

#### 4.2.2.5 Shear Strain Maps

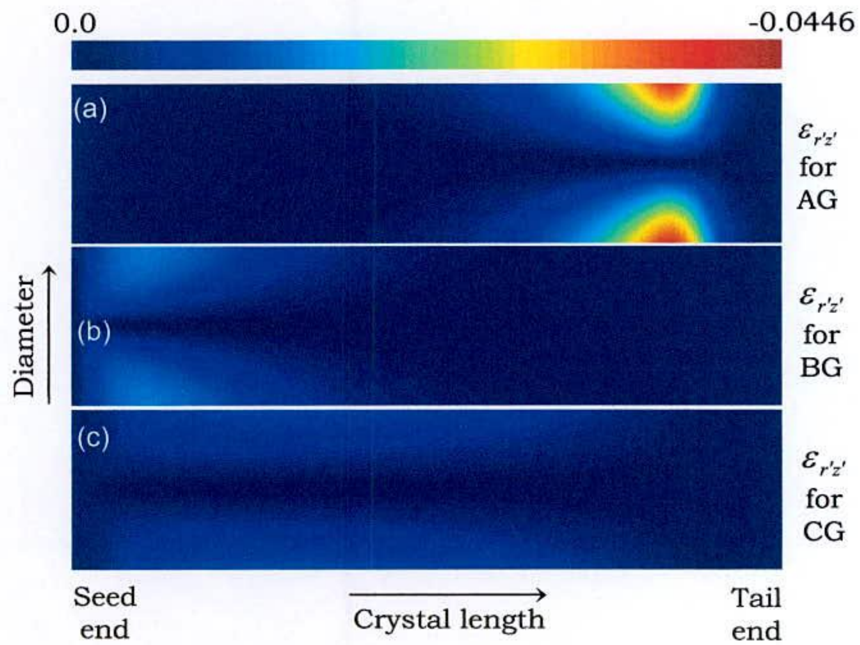


**Fig. 4.11:** Shear strain maps for the profiles AG, BG and CG

#### 4.2.2.6 Resultant Radial Strain Maps

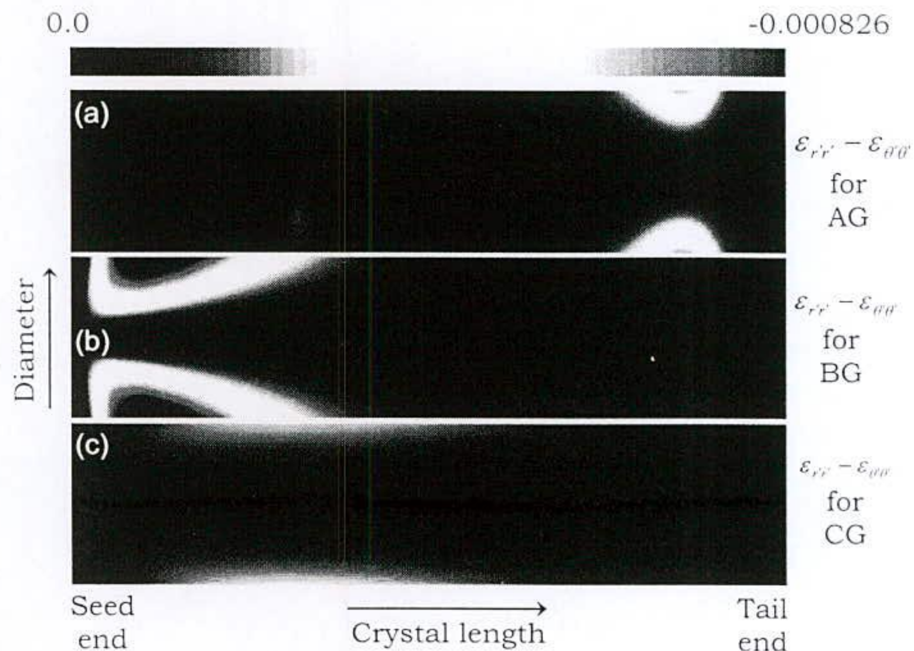


**Fig. 4.12:** Resultant radial strain maps for the profiles AG, BG and CG.

Figures 4.8, 4.9 and 4.10 show the $\varepsilon_{z'z'}$, $\varepsilon_{r'r'}$ and $\varepsilon_{\theta'\theta'}$ strain maps, respectively, for the profiles AG, BG and CG. From the color maps, it is found that these strain components show the similar strain distributions as those of the profiles AE, BE and CE along the growth direction of the crystal. However, along the radial direction, the strain distributions are found to be different than those of the previous profiles. Furthermore, the quantitative amount of strains is found to be higher at the centre than that evaluated at the periphery. This tendency of strain distribution is opposite in nature with respect to the previous profiles. This is due to the fact that the composition is higher at the centre for the profiles AG, BG and CG.

Shear strain maps are shown in Figs. 4.11(a)-(c) for the profiles AG, BG and CG, respectively. Here strain distributions are also similar to the distributions as observed previously for the profiles AE, BE and CE. Similar to the profiles AE, BE and CE, $\varepsilon_{r'z'}$ is found to be almost zero along the growth axis of the crystal for the profiles AG, BG and

CG. This result is obtained due to the axial symmetry in composition. The maximum value of $\varepsilon_{r'z'}$ for the profile AG is found around the periphery near the homogeneous composition region of the crystal. In contrast, maximum value of $\varepsilon_{r'z'}$ is found around the periphery near the seed-end of the crystal for the profile BG. On the other hand, $\varepsilon_{r'z'}$ is found to be increased gradually along the radial direction of the crystal for the profile CG. It is found from the Figs. 4.11(a)-4.11(c) that the shear strain reduces to zero for all the profiles when the composition becomes homogeneous. It is also found that the amounts of $\varepsilon_{r'z'}$ are comparatively lower for the profiles AG, BG and CG than those evaluated for the profiles AE, BE and CE.

Up to now, strain maps have been analyzed for both axial and radial variations of composition only to demonstrate the behavior of spatial distributions of strains and their quantitative amounts. But it is to be mentioned here that our aim is to grow bulk InGaAs crystals having homogeneous composition. In that case, radial asymmetry of composition is undesirable. However, since composition is increased at the initial stage of the MCZM growth process, the variation of composition along the growth direction must be considered. Hence, in the next section we will focus our further analysis on strain maps corresponding to the profiles AF, BF and CF, where the compositional variation along the radial direction is uniform.

### 4.2.3 Maps for the Profiles AF, BF and CF

#### 4.2.3.1 Composition Maps

Figures 4.13(a)-4.13(c) show composition maps, which are constructed corresponding to the compositional profiles AF, BF, and CF. Compositional variations along the growth and radial directions are shown by colors in Figs. 4.13(a)-(c).

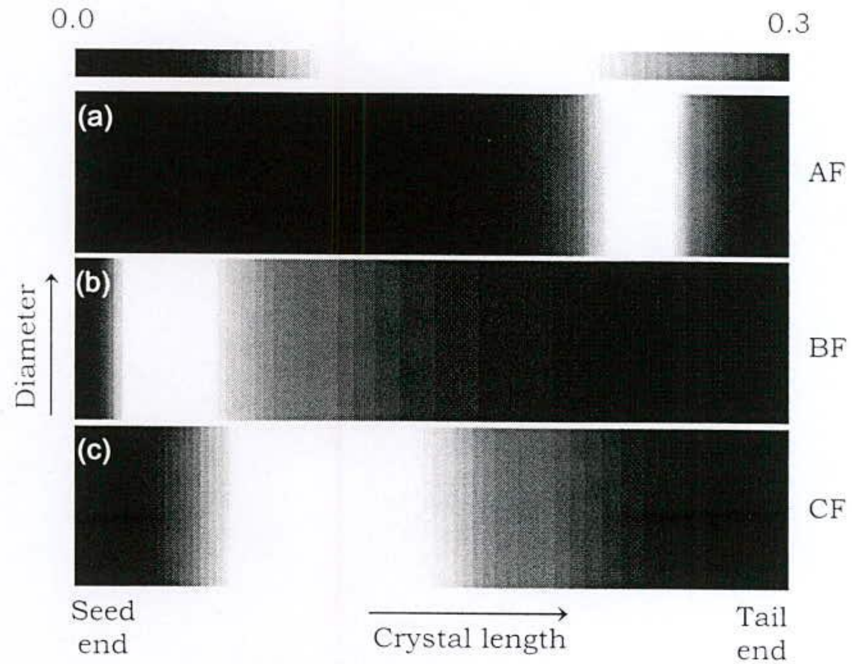


**Fig. 4.13:** Composition maps for the profiles AF, BF and CF.

### 4.2.3.2 Axial Strain Maps

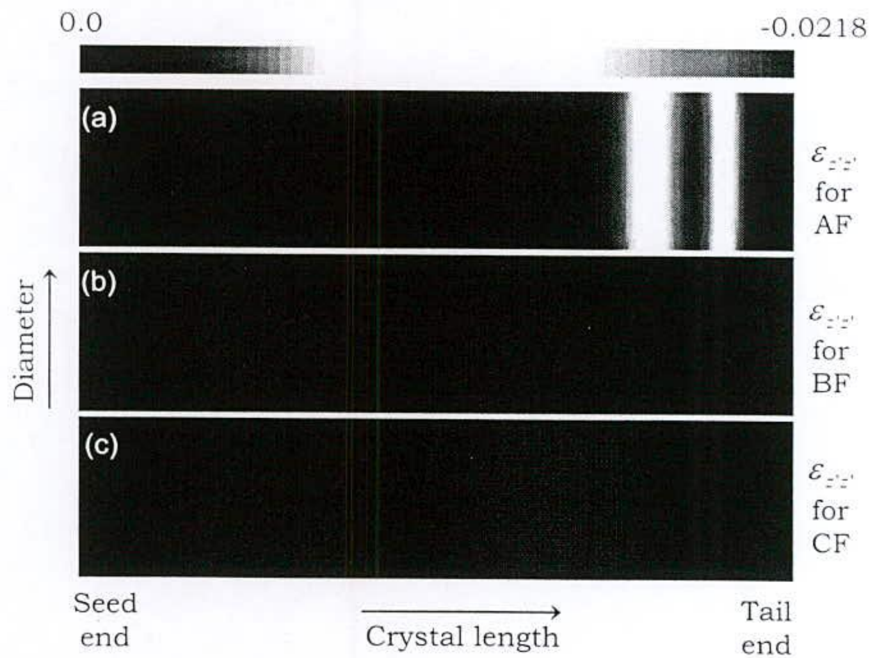


**Fig. 4.14:** Axial strain maps for the profiles AF, BF and CF.

#### 4.2.3.3 Radial Strain Maps

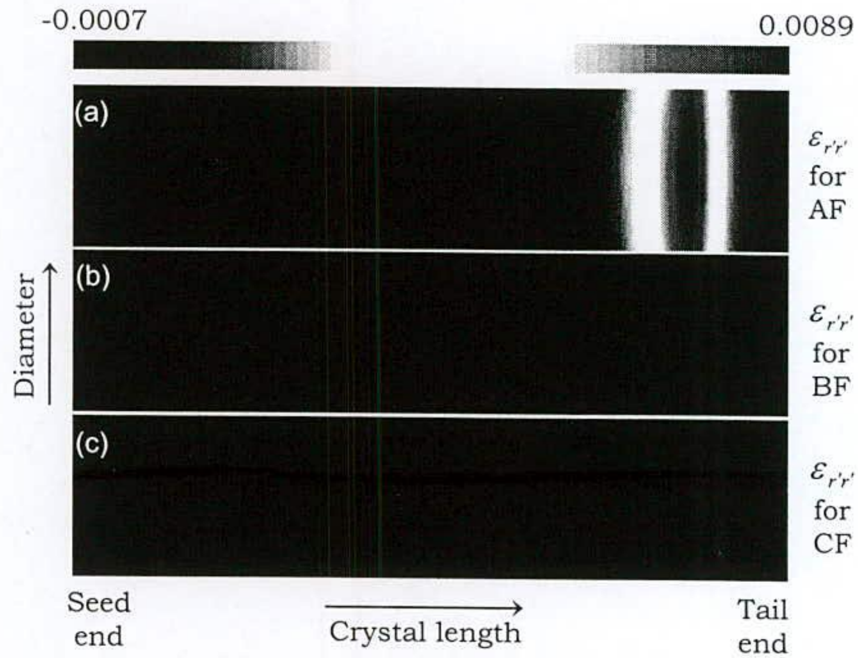


**Fig. 4.15:** Radial strain maps for the profiles AF, BF and CF.

#### 4.2.3.4 Tangential Strain Maps

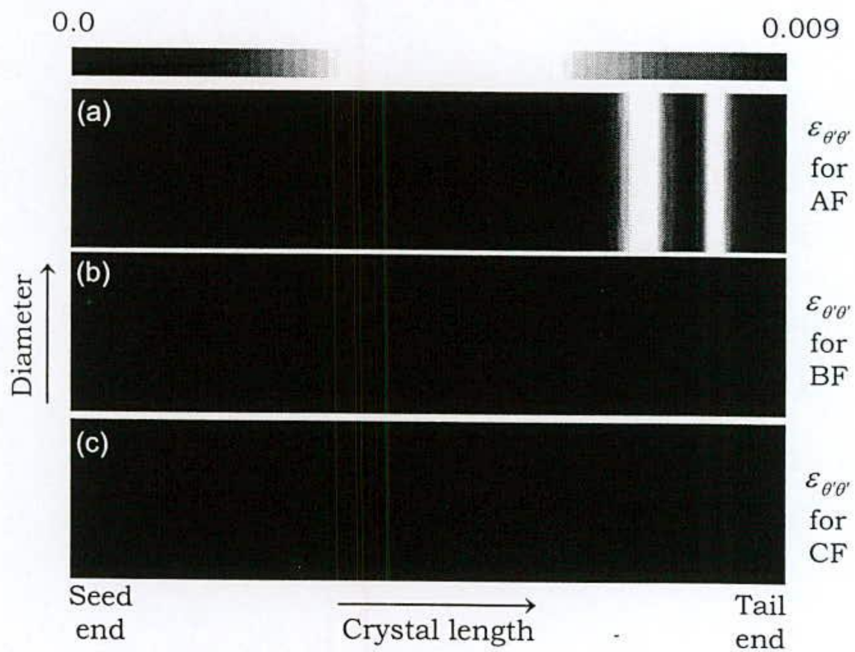


**Fig. 4.16:** Tangential strain maps for the profiles AF, BF and CF.

#### 4.2.3.5 Shear Strain Maps

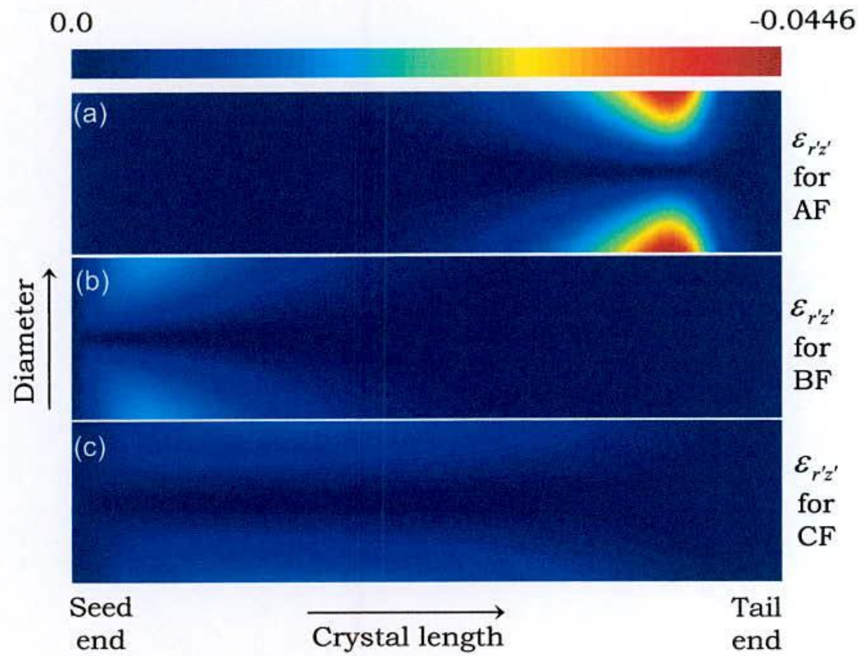


**Fig. 4.17:** Shear strain maps for the profiles AF, BF and CF.

#### 4.2.3.6 Resultant Radial Strain Maps

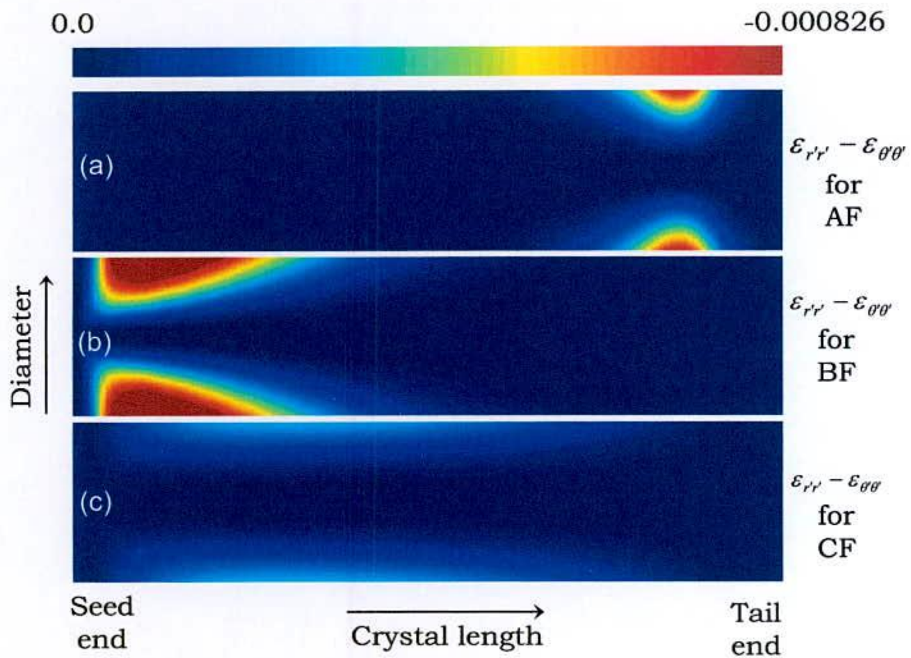


**Fig. 4.18:** Resultant radial strain maps for the profiles AE, BE and CE.

The $\varepsilon_{z'z'}$, $\varepsilon_{r'r'}$ and $\varepsilon_{\theta'\theta'}$ strain maps corresponding to the profiles AF, BF and CF are shown in Figs 4.14-4.16. It is found that the strain distributions along the growth direction are almost similar for these three principal strain components. For the profile AF, the amount of $\varepsilon_{z'z'}$, $\varepsilon_{r'r'}$ and $\varepsilon_{\theta'\theta'}$ are found to be accumulated gradually along the growth direction and then increased drastically to its maximum value near the end of the first step growth process. The strain values are suddenly reduced to zero at the end of the first step growth because of compositional homogeneity. In the case of the profile BF, these strain values accumulate rapidly near the seed-end of the crystal and then decrease gradually along the growth direction due to the gradual change in composition. In contrast, the $\varepsilon_{z'z'}$, $\varepsilon_{r'r'}$ and $\varepsilon_{\theta'\theta'}$ strain values accumulate gradually up to the 60% crystal length and then reduce to zero at the end of the first step growth process for the profile CF.

Figure 4.17 shows the shear strain maps for the profiles AF, BF and CF. It is found from the maps that the strain distributions are not the same along the radial and growth directions for the profiles AF, BF and CF, which is resulted from the rate of change in composition for these profiles. It is also found from Fig. 4.17(a)-(c) that the amount of $\varepsilon_{r'z'}$ is lower for the profile CF than those evaluated for the profiles AF and BF. Figure 4.18 shows the resultant radial strain maps for the profiles AF, BF and CF. It is found from a comparison among the Figs. 4.18(a)-(c) that the lattice deformation along the radial direction is lower in case of the profile CF than those obtained for the profiles AF and BF. Comparing the strain distributions and their quantitative value among the profiles AF, BF and CF, a suitable compositional profile has been proposed in the next section for the MCZM growth technique.

## 4.3 Selection of Suitable Profile

Analyzing the two-dimensional spatial variation of strain, it has already been understood that the strain distributions and their quantitative amounts are strongly dependent on the compositional profile and its range. It is therefore very important to find out a suitable profile which will enable us to grow high quality bulk InGaAs crystal using the two-step MCZM method. In order to do so, two-dimension strain maps plotted for various profiles have been used. Since our objective is to grow crystals with homogeneous composition, strain maps obtained for the profiles AF, BF and CF should be considered.

Investigating of the strain distributions by the line diagram as well as by the color maps corresponding to the profiles AF, BF, and CF reveal that the strain values are the highest at the end of the first step growth for the profile AF. A drastic change in strain values are also obtained near the end of the first step growth for this profile. Such a sudden change in strain degrades the crystal quality and leads to broken the crystal. It has already been mentioned that the profile used in the two-step MCZM growth process is alike the profile AF. Thus, the results obtained from the present study clearly explain the crystal breakage mechanisms in the MCZM growth process. It is believed that if any profile other than AF is used, this breakage issue can be solved. In case of the profiles BF and CF, it is found that the strain values are much lower than those obtained for the profile AF. Particularly, the strain values are almost negligible near the end of the first step growth for the profiles BF and CF. Hence both BF and CF can be considered as better profiles than the profile AF. It is found that the composition in the profile BF increases drastically near the seed-end and gradually near the end of the first step growth. Consequently, a drastic change in lattice constant leads to induce higher values of strain near the seed-crystal interface. This higher values of strain then decrease rapidly because of the behavior of the profile BF. The crystal may be

broken due to this drastic change in strains near the seed region. Thus, it can be concluded that the profile BF would not be suitable for the growth of high quality InGaAs crystal using the MCZM method.

In contrast to the profiles AF and BF, the composition in the profile CF increases almost linearly along the growth direction. Due to this linear change in composition, the strain values are increased gradually along the radial and growth directions until 60% of the crystal length for the profile CF. After that the values of strain start decreasing while moving towards the homogeneous composition region of the crystal where the first step growth has been completed. When the composition becomes uniform ($x \sim 0.3$), the strain values are almost negligible for the profile CF. Thus, comparing the strain distributions and their magnitudes evaluated corresponding to the profiles AF, BF and CF, it can be concluded that if the profile CF is used in the MCZM growth process, high quality bulk InGaAs crystal can be expected. In order to investigate the state of strain with crystal length and diameter for the profile AF, strain maps have been further developed and shown in the next section.

## 4.4 Dependence of Strain with Crystal Length

Spatial variation of strains by changing the crystal length has been investigated here for the profile CF. Figure 4.19 shows the color maps for various strain components corresponding to the crystals of 30 mm and 50 mm lengths with 15 mm diameter. Color maps corresponding to the 30 mm and 50 mm long crystals are arranged in two different columns in Fig 4.19. It is found from Fig. 4.19 that the axial, radial and tangential strain distributions and their magnitudes are almost the same for the two crystals. Although the strain values are found to be independent with the crystal length, the accumulation rate of strain is higher for the shorter crystal than that of the longer crystal. Shear and resultant radial strain values show some variations with

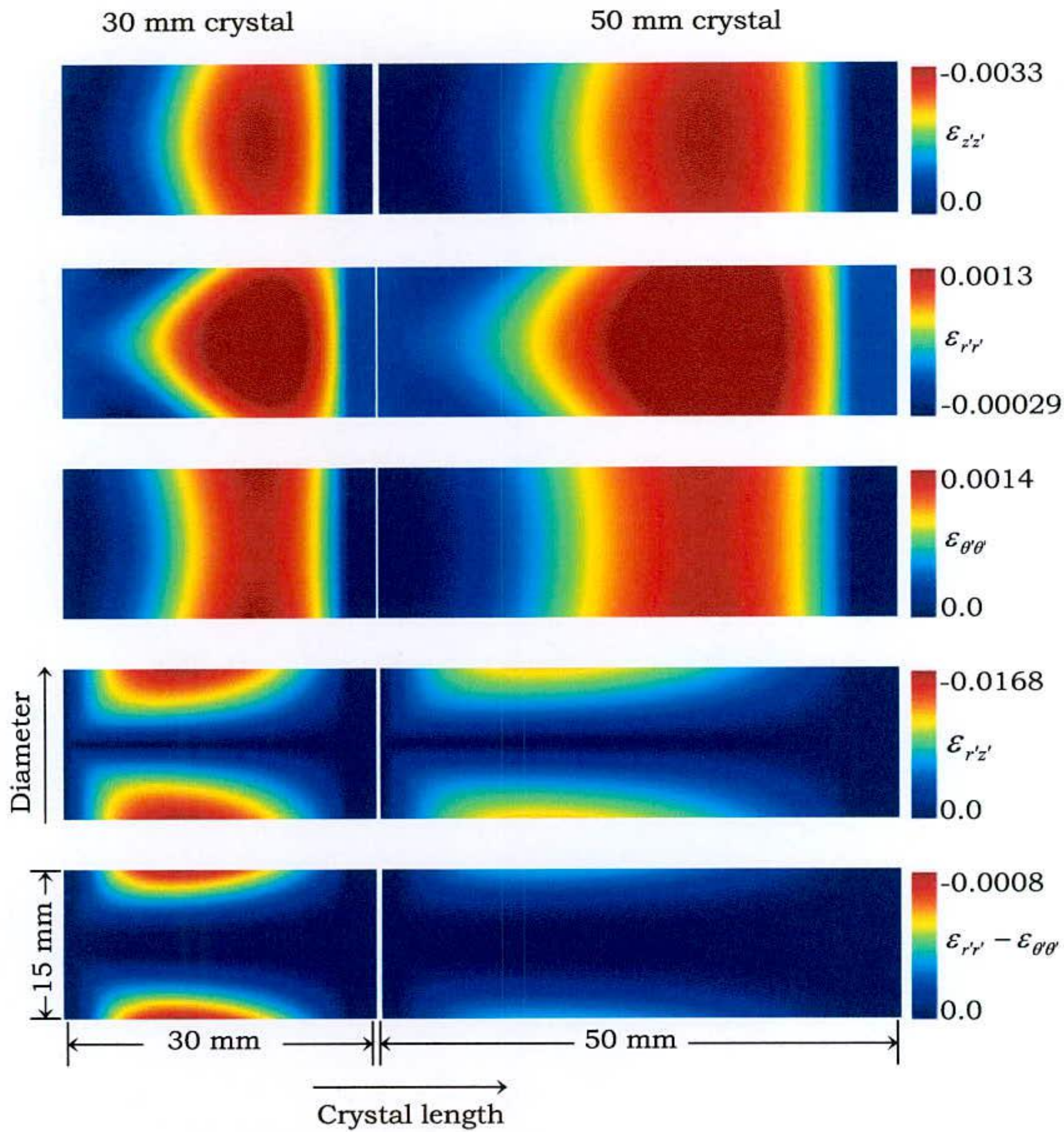


**Fig 4.19:** Strain distributions of two crystals having 30 mm and 50 mm length with the same diameter (15 mm).

respect to the crystal length though the distributions are similar for both cases. Crystal with longer length shows lower shear and resultant radial strain values than those of the shorter crystal. Thus, if the length of the crystal in the first step of the MCZM growth process is increased, quality of the crystal can be improved. Since it is our main objective to grow large size high quality InGaAs crystal using

MCZM method, the dependence of strain values with the crystal diameter has been investigated further in the next section.

## 4.5 Dependence of Strain with Crystal Diameter

Figure 4.20 shows the color maps corresponding to various strain components for the compositional profile CF. the strain maps are constructed for the two different diameters of 15 mm and 20 mm while the crystal length was 30 mm. The color maps corresponding to the 15 mm and 20 mm diameter crystals are arranged in two different columns as shown in Fig 4.20. The axial, radial and tangential strain distributions and their magnitudes are found to be almost independent with the crystal diameter as indicated in Fig. 4.20. In the case of the shear and resultant radial strains, it is clearly observed that the strain distribution does not change with the diameter. However, the quantitative amount of strain is found to be higher when diameter is increased from 15 mm to 20 mm. Thus growth of large diameter crystal may degrade crystal quality due to increase in shear strain components.

Further analysis has been carried out to investigate the possibility of growing larger diameter crystals by the MCZM method. It is found from the previous discussions that the shear strain, which is mainly responsible for the crystal breakage, has a strong dependence with crystal diameter and length. It is expected that large diameter crystal can be obtained if the crystal length in the first step of growth process of two-step MCZM method is increased. To understand this possibility, color strain maps are plotted for the profile CF for two different crystals of 30 mm in length and 20 mm in diameter and 60 mm in length and 25 mm in diameter. The results are summarized in Fig. 4.21, where color maps obtained for the two different crystals are arranged in two different columns with a normalized color scale. It is clearly observed that the distributions for all the strain components

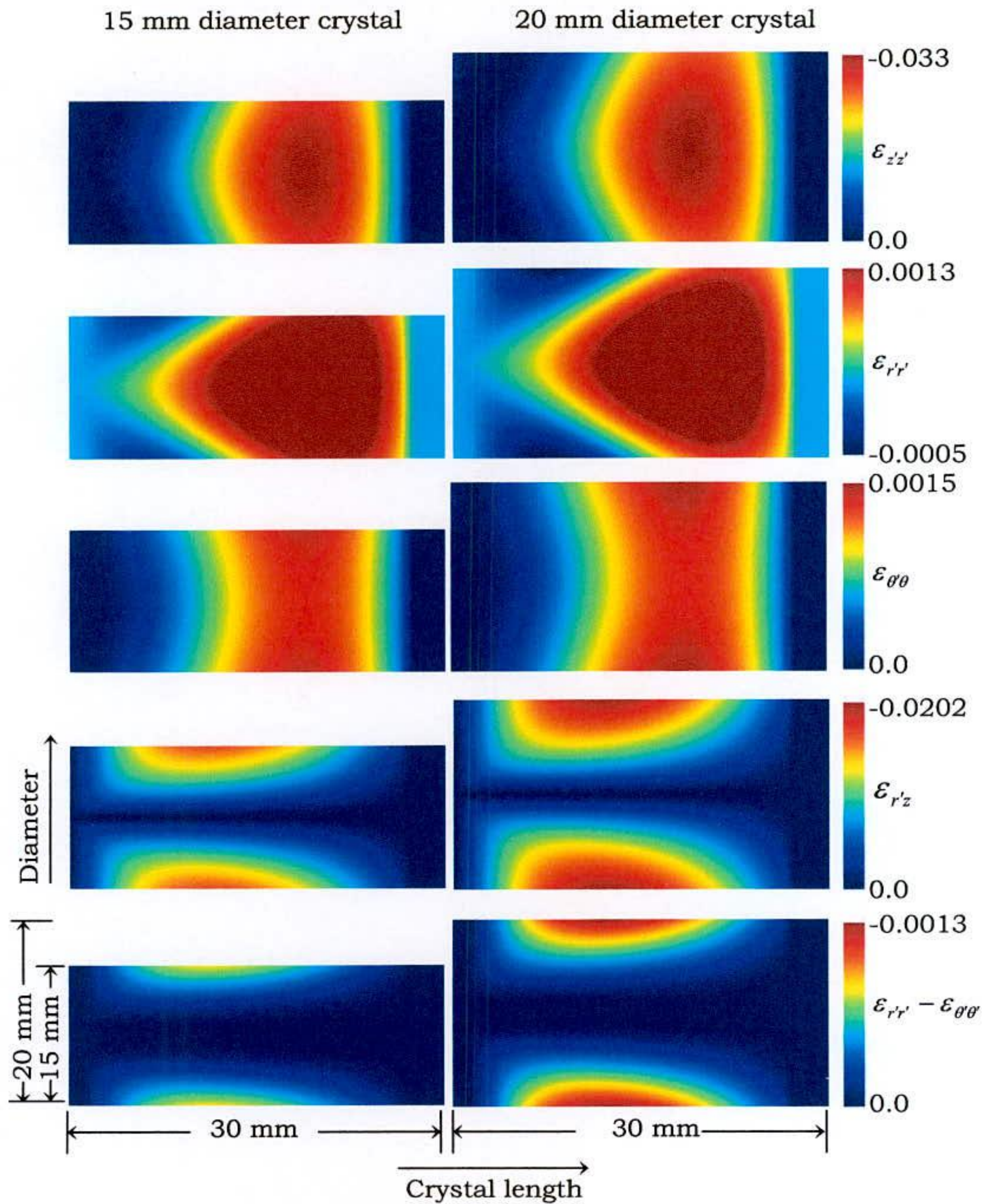


**Fig 4.20:** Strain distributions of two crystals having 20 mm and 15 mm diameter with equal length of 30 mm.

are almost same for the two different crystals. The $\varepsilon_{z'z'}$, $\varepsilon_{r'r'}$ and $\varepsilon_{\theta'\theta'}$ strain components are slightly increased with the crystal length and diameter. However, if the diameter is increased from 15 mm to 20 mm, shear and resultant radial strains are increased for the same

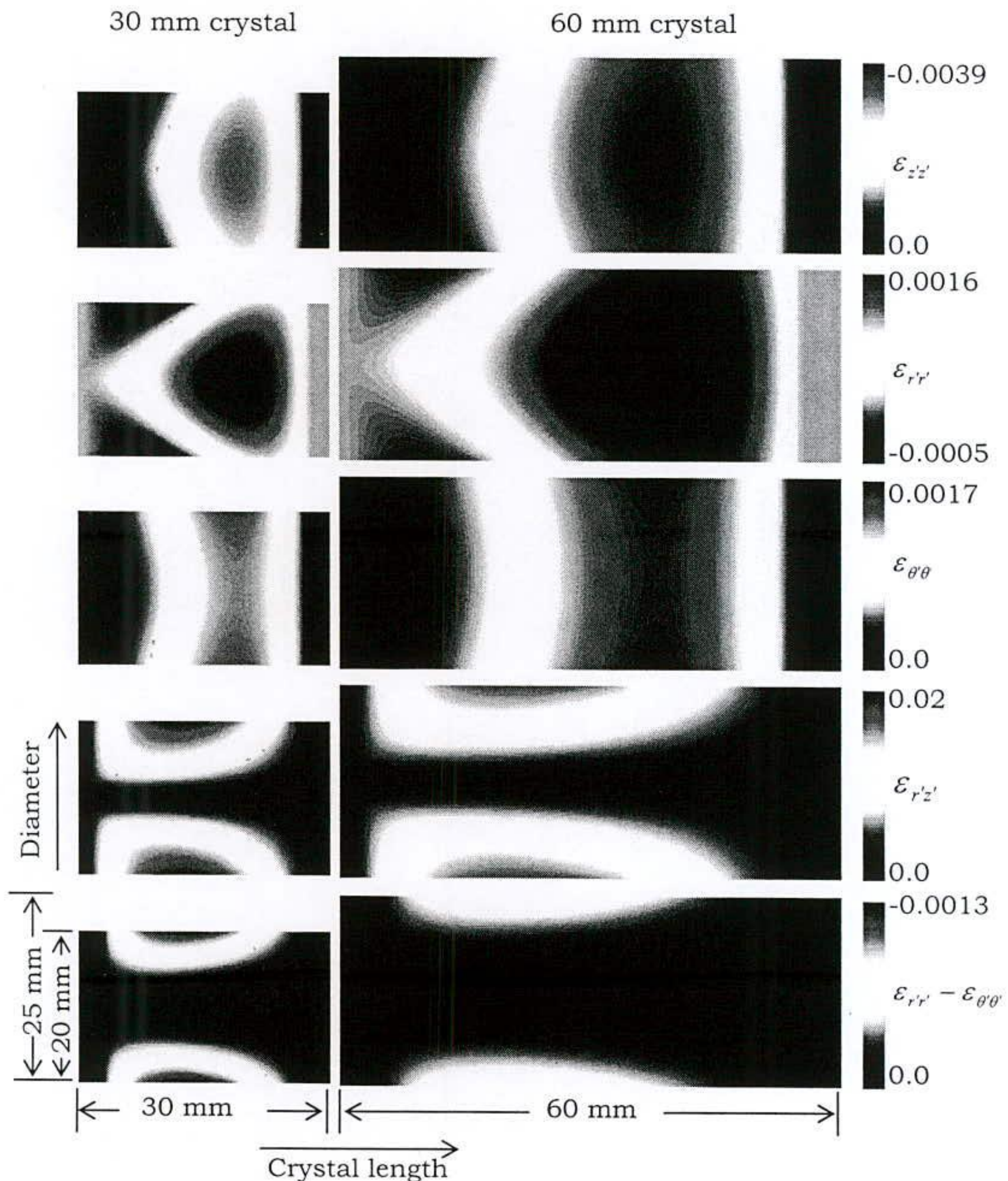


**Fig 4.21:** Strain distributions of two crystals having 30 mm length and 20 mm diameter and 60 mm length and 25 mm diameter.

crystal length as discussed in Fig. 4.20. Conversely, it is observed from Fig. 4.21 that, if the crystal length is sufficiently increased, then the shear and $\varepsilon_{r'r'} - \varepsilon_{\theta'\theta'}$ strain values are decreased significantly even the crystal diameter is increased from 20 mm to 25 mm. Therefore, from the above discussions it can be concluded that high quality

InGaAs crystals with larger diameter can be obtained if the crystal length is sufficiently increased in the first-step growth of the two-step MCZM growth process.

## 4.6 Temperature Profile

It is found from the InGaAs phase diagram that the compositional profile in InGaAs crystal can be controlled by controlling the temperature at solid-liquid interface. The solidification temperature as a function of the composition can be obtained by the following relationship [34]

$$T_S = 1235.18 - 1448.33x + 3391.55x^2 - 3627.43x^3 + 1392.77x^4 \quad (4.1)$$

Using the existing-like (AF) and the proposed-like (CF) compositional profiles, the solidification temperature profiles are evaluated by

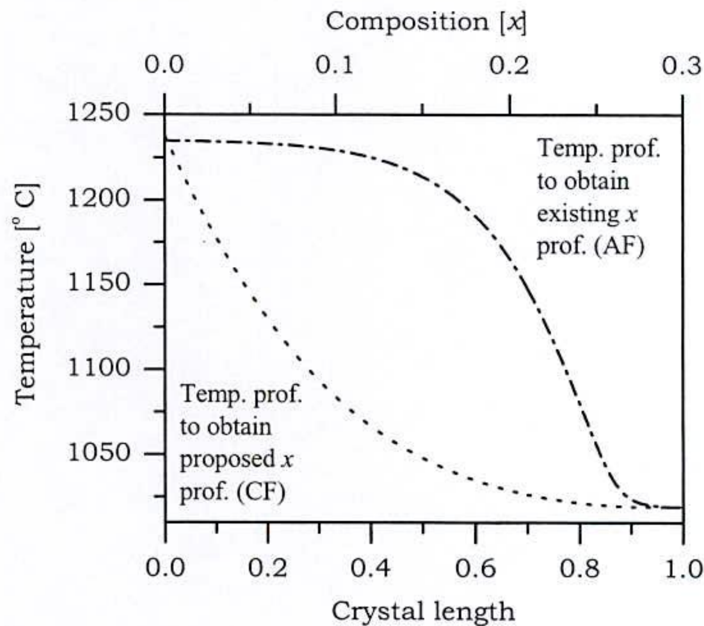


**Fig. 4.22:** Solidification temperature profiles as a function of composition as well as normalized crystal length for the existing-like (AF) and proposed-like (CF) compositional profiles.

Eq.(4.1). The results are shown in Fig. 4.22 as a function of the composition as well as normalized crystal length. It is observed in Fig. 4.22 that the slope of the temperature profile evaluated corresponding to the existing-like compositional profile (AF) changes drastically from 40% to 95% crystal length in one direction and then changes dramatically in opposite direction within 95% to 100% crystal length in the first step growth process. Such a change in temperature is very difficult to achieve physically in the furnace. On the other hand, the slope of the temperature profile estimated corresponds to the proposed-like compositional profile (CF) changes almost linearly in the first step growth process, which is easily attainable. Thus proposed compositional profile leads to obtain growth parameters easily and hence enable us to grow high quality large size bulk InGaAs crystals using the two-step MCZM method.

## 4.7 Summary

In order to observe the spatial variations of residual strains induced due to the compositional variation and hence to understand the breakage issue in bulk InGaAs crystals grown by the MCZM process, a two-dimensional mapping of composition and strain has been developed. Strain maps have been constructed for the nine different compositional profiles. Analyzing the color maps for the various strain components corresponding to the compositional profiles under consideration, it is found that the highest values of strains are accumulated near the homogeneous composition region for the profiles AF, AE and AG, which are similar to the existing-like compositional profile. This is due to the large change in lattice spacing at this region. For the profiles AG, BG and CG the strain values are found to be the highest near the seed-end of the crystal. On the other hand, highest values of strains are found at approximately 60% of the crystal length, for the profiles AF, BF and CF. In order to choose the suitable compositional profile, spatial variations of strains are

analyzed from the color maps for the profiles AF, BF and CF. The quantitative amount of the strains, particularly, the shear and resultant radial strain, for the profile AF is found to be much higher than those of the profiles BF and CF. The higher value of shear strain may be the cause of crystal breakage. Hence, it is expected that the profiles BF and CF would give high quality crystal in MCZM growth process due to accumulation of lower amount of strains. It is also observed that strain accumulation for the profile BF is higher at the seed-end due to the large change in composition at this region. On the other hand, change in strain is found to be gradual throughout the crystal for the profile CF. Hence, the profile CF is proposed to be the best compositional profile to be used in the MCZM growth technique. Furthermore, investigations are done to examine the possibility of growing large diameter crystal. It is found that the shear strain component, which is the main cause of crystal breakage, is increased with increasing crystal diameter and length. It is also found that if the crystal length in the first-step of the MCZM growth process is sufficiently increased, the shear strain would be considerably reduced and growth of larger diameter crystal would be possible by the MCZM growth technique. Additionally, it is investigated that the proposed profile enables us to obtain growth parameters easily than the existing profile.

Chapter 5

# Conclusions and Suggestions

## 5.1 Conclusions

In this thesis, following research aspects have been reported: (1) experimental investigation of residual strain in bulk $In_xGa_{1-x}As$ mixed crystals grown by the MCZM method and hence to reveal the breakage issue, (2) analysis of strain components for various compositional profiles using an axially symmetrical strain model, (3) development of two-dimensional composition and strain maps to investigate the spatial variations of composition and strain in bulk InGaAs crystals, (4) selection of best compositional profile to solve the crystal breakage problem in two-step MCZM growth process (5) investigation of the dependency of strain values with the crystal length and diameter, (6) suggestion of suitable growth parameters for the two-step MCZM growth method.

Existence of residual strain in bulk InGaAs crystals grown by the two-step MCZM method has been confirmed by means of RS and PL experiments in conjunction with EDX experiment. Comparing the RS, PL and EDX results it was found that $TO_{GaAs}$ and PL peak positions were changed under the influence of strain. The strain-induced shift in phonon position was 4.04 $cm^{-1}$ and the PL peak energy was changed by 0.097 eV for the variation of composition from 0.06 to 0.29. Further, the line shape of $TO_{GaAs}$ phonon was broadened rapidly 2.99 $cm^{-1}$ near the seed-crystal interface due to the drastic change in composition from 0 to 0.06. For the gradual increment of

composition from 0.06 to 0.29, the lineshape was increased gradually from 9.68 $cm^{-1}$ to 12.93 $cm^{-1}$. Such a large strain-induced shifts in $TO_{GaAs}$ phonon and PL peak positions as well as the broadening of $TO_{GaAs}$ lineshape demonstrate that there exists huge amount of strain in the order of $10^{-2}$ due to the compositional variation in bulk InGaAs crystals grown by the two-step MCZM method.

In order to determine the quantitative amount of strains and their distributions in bulk InGaAs crystals for various typical compositional profiles, an axially symmetrical strain model has been applied. Strain distributions have been calculated for nine different compositional profiles, which can be used in the first step growth of the two-step MCZM growth process. It is found from the strain distributions that the strain components are dependent on the shape the compositional variations and range of composition. In case of the compositional profiles AF, AE and AG, which are similar to the compositional profile currently being used in the first step growth of the two-step MCZM growth technique, the strain values were found to be increased gradually near the seed-end due to gradual increment in composition. However, the strain values are found to be increased rapidly at the end of the first step growth process due to the drastic change in composition. This drastic change in strain values explains the crystal breakage phenomenon in the two-step MCZM growth process. Further, from the strain distributions for the profiles BF, BE and BG, it was found that the stain values are increased considerably at the seed-end of the crystal and these were gradually reduced to zero at the end of the first step MCZM growth process. On the other hand, the compositional profiles CF, CE and CG showed gradual increase in strain values up to 60% crystal length and then the strain values gradually reduced to zero at the end of the first step growth process. By comparing the quantitative amount of strains evaluated for various compositional profiles, the lower values of strain are found for the profiles CF, CE and CG. Hence, these three profiles would give better

results in the MCZM growth process. Since our aim is to grow compositionally homogeneous InGaAs crystals, the profile having flat radial distribution such as the profile CF would be desirable.

In order to observe the spatial variation of strain for various compositional profiles and hence to determine the best profile for the two-step MCZM growth process, further two-dimensional composition and strain maps have been developed. From the color maps of strains for the profiles AF, AE and AG, it was found that the highest values of strains were accumulated near the periphery of the crystal at the end of the first step growth process. However, the highest values of strains were found near the seed-end of the crystal for the profiles BF, BE and BG. On the other hand, strain values were found to increase gradually up to a certain crystal length and then reduced to zero at the end of the first step growth process for the profiles CF, CE and CG. Furthermore, the Profiles CF, CE and CG shown lower values of strains compared to those of the other profiles. Comparing the strain values and their distributions for all the profiles it was concluded that the profile CF is the best compositional profile for the two-step MCZM growth process concerning the breakage issue.

The dependence of the strain values with crystal length and diameter were also investigated by the two-dimensional color maps. The axial, radial and tangential strains are found to have negligible dependency with the crystal length and diameter, although there is a strong dependency of the shear and resultant radial strains with them. Further, it has been found that if the crystal length in the first-step of the MCZM growth process is sufficiently increased, the shear strain would be considerably reduced and growth of larger diameter crystals would be possible by the two-step MCZM growth technique.

Additionally, solidification temperature profiles which are required to obtain the existing and proposed compositional profiles have been estimated and compared. It has been found that it is easier

to achieve the growth parameters, for the proposed compositional profile than the existing profile.

## 5.2 Suggestions for future works

In this work, the strain models have been applied by assuming axial symmetry in composition in isotropic materials, which can be extended further to investigate strain distributions in anisotropic conditions for any compositional profile in bulk InGaAs crystals. Taking temperature effect into consideration, new strain models can be developed further for understanding various issues associated with the growth of bulk InGaAs crystals.

In order to obtain compositionally homogeneous high-quality InGaAs crystals, solidification temperature should be maintained accurately according to the proposed temperature profile. It is therefore very important to develop precise temperature measurement techniques by setting thermocouples inside the melt. Having the appropriate growth parameters, further growth experiments can be carried out considering the compositional profile, which has been suggested in the present study for the two-step MCZM growth method.

# Bibliography

[1] Communication White Paper, 1992, 1996, Ministry of International Trade and Industry, Tokyo.

[2] T. Miki, "Optical transport networks", Proc. IEEE, vol. 81, no. 11, pp. 1594-1609, 1993.

[3] R. Gangopadhyay, M. R. Islam, S. P. Majumder and B. Pal, "Performance evaluation of a WDM ring network employing CPFSK transmission in the presence of GVD and SPM", J. Optical commun. vol. 20, no. 4, pp. 138-144, 1999.

[4] M. Kaneko, S. Nakayama, K. Kashiwa, S. Aizawa and N. S. Takahashi, "Lattice mismatched LPE growth of InGaP on patterned InP substrate", Cryst. Res. Technol., vol. 37, no. 2-3, pp. 177-182, 2002.

[5] H. Ishikawa, "Theoretical gain of strained quantum well grown on an InGaAs ternary substrate", Appl. phys. Lett., vol. 63, no. 6, pp. 712-714, 1993.

[6] K. Otsubo, Y. Nishijima, T. Uchida, H. Shoji, K. Nakajima and H. Ishikawa, "1.3 μm InGaAs/InAlGaAs strained quantum well lasers on InGaAs ternary substrates", Jpn. J. Appl. Phys., vol. 38, Part 2, no. 3B, pp. L312-L314, 1999.

[7] W. A. Bonner, B. J. Skromme, E. Berry, H. L. Gilchirst and R. E. Nahory, *15th Intl. Symp. on GaAs and Related Compounds*, Atlanta, GA, 337, (1988), edited by J. S. Harris. Inst. Phys. Conf. Ser. 96 , Bristol: Inst. Phys., 1989.

[8] K. Nakajima and T. Kusunoki, "Constant temperature LEC growth of InGaAs ternary bulk crystals using the double

crucible method", J. Cryst. Growth, vol. 169, no. 2. pp. 217-222, 1996

[9] K. Nakajima, T. Kusunoki and K. Otsubo, "Bridgman growth of compositionally graded $In_xGa_{1-x}As$ ($x$ = 0.05–0.30) single crystals for use as seeds for $In_{0.25}Ga_{0.75}As$ crystal growth", J. Cryst. Growth, vol. 173, no. 1-2, pp. 42-50, 1997.

[10] Y. Nishijima, K. Nakajima, K. Otsubo and H. Ishikawa, "InGaAs single crystal using a GaAs seed grown with the vertical gradient freeze technique", J. Cryst. Growth, vol. 197, no. 4, pp. 769-776, 1999.

[11] K. Kinoshita, H. Kato, M. Iwai, T. Tsuru, Y. Muramatsu and S. Yoda, "Homogeneous $In_{0.3}Ga_{0.7}As$ crystal growth by the traveling liquidus-zone method", J. Cryst. Growth, vol. 225, no. 1, pp 59-66, 2001.

[12] T. Suzuki, K. Nakajima, T. Kusunoki and T. Kato, "Multi-component zone melting growth of ternary InGaAs bulk crystal", J. Electron. Mater., vol. 25, no. 3, pp. 357-361, 1996.

[13] S. Kodama, Y. Furumura, K. Kinoshita, H. Kato and S. Yoda, "Single crystalline bulk growth of $In_{0.3}Ga_{0.7}As$ on GaAs seed using the multi-component zone melting method", J. Cryst. Growth, vol. 208, no. 1-4, pp. 165-170, 2000.

[14] M. R. Islam, A. Hiroki and M Yamada, "Modeling and analytical calculation of strain induced by gradual variation of composition in bulk $In_xGa_{1-x}As$ mixed crystal", Jpn. J. Appl. Phys., vol. 43, no. 3, pp. 1088-1093, 2004.

[15] M. R. Islam, P. Verma, M. Yamada, M. Tatsumi and K. Kinoshita, "Micro-Raman characterization of starting material for traveling liquidus zone growth method", Jpn. J. Appl. Phys., vol. 41, Part 1, no. 2B, pp. 991-995, 2002.

[16] M. R. Islam, P. Verma, M. Yamada, S. Kodama, Y. Hanaue and K. Kinoshita, "The influence of residual strain on Raman scattering in $In_xGa_{1-x}As$ single crystals", Mater. Sci. Eng., vol. B91-92, pp. 66-69, 2002.

[17] M. R. Islam, M. Yamada, N. V. Abrosimov, M. Kiyama, and M. Tatsumi, "Raman scattering characterization of residual strain and alloy composition in bulk $Si_{1-x}Ge_x$ crystal", Eur. Phys. J. Appl. Phys., vol. 27, pp. 325-328, 2004.

[18] M. R. Islam, M. Suzuki, P. Verma, M. Yamada, M. Tatsumi, Y. Hanaue and K. Kinoshita, "Two-dimensional mapping of composition in bulk $In_xGa_{1-x}As$ crystals using photoluminescence", 12$^{th}$ International Conference on Semiconducting and Insulating Materials, Smolenice Castle, Slovakia, IEEE Catalog No: 02CH37343, pp. 194-197, 2002.

[19] N. Usami, T. Takahashi, K. Fujiwara, T. Ujihara, G. Sazaki, Y. Murakami and K. Nakajima, "Evidence of the presence of built-in strain in multicrystalline SiGe with large compositional distribution", Jpn. J. Appl. Phys., vol. 41, Part 1, no. 7A, pp. 4462-4465, 2002.

[20] M. Cardona, *Light Scattering in Solids*, 2$^{nd}$ Edition, Springer-Verlag, Berlin 1, 1983.

[21] J. P. Estrera, P.D. Stevens, R. Glosser, W. M. Duncan, Y. C. Kao, H. Y. Liu and E.A. Beam, "Phonon mode study of near-lattice-matched $In_xGa_{1-x}As$ using micro-Raman spectroscopy", Appl. Phys. Lett., vol. 61, no. 16, pp. 1927-1929, 1992.

[22] J. Groenen, G. Landa, R. Carles, P. S. Pizani and M. Gendry, "Tensile and compressive strain relief in $In_xGa_{1-x}As$ epilayers grown on InP probed by Raman scattering", J. Appl. Phys., vol. 82, no. 2, pp. 803-809, 1997.

[23] M. H. Brodsky and G. Lucovsky, "Infrared reflection spectra of $Ga_{1-x}In_xAs$: A new type of mixed-crystal behavior", Phys. Rev. Lett., vol. 21, pp. 990-993, 1968.

[24] M. R. Islam and M. Yamada, "Micro-Raman scattering study of strain induced by compositional variation in single crystalline $Si_{1-x}Ge_x$ discs", Post Conference Proc. of International Symposium on Compound Semiconductors, Sandiago, California, IEEE catalog no. 03TH8767, pp. 78-83, 2003.

[25] A. Debernardi, C. Ulrich, M. Cardona and K. Syassen, "Pressure dependence of Raman linewidth in semiconductors", Phys. Stat. Sol. (b), vol. 223, no. 1, pp. 213-223, 2001.

[26] S. C. Jain, M. willander and H. Maes, "Stresses and strains in epilayers, stripes and quantum structures of III – V compound semiconductors", Semicond. Sci. Technol., vol. 11, no. 5, pp. 641-671, 1996.

[27] A. Bensaada, A. Chennouf, R. W. Cochrane, J. T. Graham, R. Leonelli and R. A. Masut, "Misfit strain, relaxation, and band-gap shift in $Ga_xIn_{1-x}P$/InP epitaxial layers", J. Appl. Phys., vol. 75, no. 6, pp. 3024-3029, 1994.

[28] T. D. Harris, M. G. Lamont, R. Sauer, R. M. Lum and J. K. Klingert, "Near-gap photoluminescence of GaAs grown directly on silicon", J. Appl. Phys., vol. 64, no. 10, pp. 5110-5116, 1988.

[29] H. Asai and K. Oe, "Energy band-gap shift with elastic strain in $Ga_xIn_{1-x}P$ epitaxial layers on (001) GaAs substrates", J. Appl. Phys., vol. 54, no. 4, pp. 2052-2056, 1983.

[30] J. M. Gilperez, F. Gonzalez-Sanz, E. Calleja, E. Munoz, J. M. Calleja, N. Mestres, J. Castagné and E. Barbier, "Photoluminescence and Raman analysis of strain and composition in InGaAs/AlGaAs pseudomorphic eterostructures" Semicond. Sci. Technol., vol. 7, no. 4, pp. 562-566, 1992.

[31] S. P. Timoshenko and J. N. Goodier, *Theory of Elasticity*, 3rd ed., McGraw-Hill, New York, 1970.

[32] M. R. Islam, P. Verma and M. Yamada, "Residual strain induced by strain in bulk $In_xGa_{1-x}As$ crystals with gradual variation in composition", *Advanced Nanomaterials and Nanodevices*, ed. Hongjun Gao, Harald Fuchs and Dongmin Chen (IOP Publishing Ltd.) Electronic Book. pp. 912-926, 2003.

(http://www.nanotechweb.org/resources/Books/)

[33] H. F. Wolf, *Semiconductors*, 1st ed, Pergamon Press, Oxford, 1968.

[34] H. Nakamura, H. Kato, K. Kinoshita and S. Yoda, NASDA Tech. Memorandum, vol. 15, 2000.

# List of Publications

[1]. **M. S. Rahman**, M. R. Islam, and M. Yamada, "Spectroscopic investigation of strain induced by compositional variation in bulk $In_xGa_{1-x}As$ crystal grown by MCZM method", accepted for publication in the Journal of Crystal Research and Technology.

[2]. M. R. Islam, R. Ahshan, **M. S. Rahman**, A. G. Bhuiyan, P. Verma, M. Yamada, and M. Tatsumi, "Preliminary Results on Crystal Growth of Bulk $InxGa1\text{-}xAs$ Using TLZ method", in proceedings of the 3rd International Conference on Electrical and Computer Engineering, December 2004, Dhaka, Bangladesh, pp. 260-263.